DESIGN AND ANALYSIS
OF
2D PHOTONIC CRYSTAL DEVICES

A Dissertation Submitted in partial fulfilment of the requirements for the award of the degree of

Master of Engineering

in

Electronics and Communication Engineering

Submitted by

Harkiranjeet Kaur

Roll No. : 801361009

Under the guidance of

Dr. R. S. Kaler

Senior Professor and Deputy Director

T.U. Patiala

ELECTRONICS AND COMMUNICATION ENGINEERING

DEPARTMENT

THAPAR UNIVERSITY

(Established under the section 3 of UGC Act, 1956)

PATIALA – 147004 (PUNJAB)

CERTIFICATE

I, Harkiranjeet Kaur, hereby declare that the work which is being presented in the dissertation entitled, **"Design and Analysis of 2D Photonic Crystal Devices"** by me in partial fulfillment of the requirement for the award of degree of M.E in Electronics and Communication submitted in Electronics and Communication Engineering Department of Thapar University, Patiala is an authentic record of my own work carried out under the supervision of **Dr. R. S. Kaler**, Senior Professor, ECED.

The matter presented in this dissertation has not been submitted in any other University/Institute for the award of degree.

Date: July 01, 2015

HARKIRANJEET KAUR
ROLL NO: 801361009

It is certified that the above statement made by the student is correct to the best of my knowledge and belief.

Date: July 01, 2015

Dr. R. S. Kaler
Senior Professor & Deputy Director
Thapar University

Countersigned By:-

Dr. Sanjay Sharma
Professor & Head
ECED, Thapar University

Dr. S.S. Bhatia
Dean of Academic Affairs
Thapar University

ACKNOWLEDGEMENT

To discover, analyze and to present something new is to venture on an untrodden path towards and unexplored destination is an arduous adventure unless one gets a true torch bearer to show the way. I would have never succeeded in completing my task without the cooperation, encouragement and help provided to me by various people. Words are often too less to reveals one's deep regards. I take this opportunity to express my profound sense of gratitude and respect to all those who helped me through the duration of this thesis. I acknowledge with gratitude and humility my indebtedness to **Dr. R. S. Kaler, Senior Professor,** Electronics and Communication Engineering Department, Thapar University, Patiala, under whose guidance I had the privilege to complete this thesis. I wish to express my deep gratitude towards him for providing individual guidance and support throughout the dissertation work.

I convey my sincere thanks to **Head of the Department, Dr. Sanjay Sharma** as well as **PG Coordinator, Dr. Amit Kumar Kohli, Associate Professor,** Electronics and Communication Engineering Department, entire faculty and staff of Electronics and Communication Engineering Department for their encouragement and cooperation.

My greatest thanks are to all who wished me success especially my parents. Above all I render my gratitude to the almighty who bestowed self-confidence, ability and strength in me to complete this work for not letting me down at the time of crisis and showing me the silver lining in the dark clouds. I do not find enough words with which I can express my feelings of thanks to my dear friends and seniors for their help, inspiration and moral support which went a long way in successful competition of the present study.

Harkiranjeet Kaur

Roll No. 801361009

ABSTRACT

In the recent few years, the photonic crystals have provided a potential platform for a wide range of applications in numerous domains. Many optical communication devices such as multiplexers/de-multiplexers, interleavers, filters etc., designed on the photonic crystals have been reported showing high throughputs. These devices have made a significant contribution in the areas of compactness, miniature sizes and fast switching etc. The photonic crystals are periodic dielectric structures which compose of alternate high and low refractive index materials. The refractive index repeats after certain period which is of the order of the wavelength of light. So, when the light waves traverse these crystals, it suffers the multiple reflections resulting in either destructive or constructive interference. The range of frequencies, due to this phenomenon becomes non permissible in the crystal. This range is known as forbidden band or photonic band gap. It is clearly visible when we plot dispersion curves of the crystal lattices.

The objective of this dissertation is to design and analyze various guiding optical circuits based on the two dimensional photonic crystals. The dispersion curves of the circuits are studied with the help of Plane-Wave Expansion (PWE) method and the band gaps are found. We then create a number of point and line defects in the crystal to vanish these band gaps due to localization of the energy in the cavities formed by defects. This is done with the help of OPTIFDTD software. The power transmission curves for these structures are also investigated. The transmission of light can be studied with the help of Maxwell's equations. The Maxwell's equations are solved using Finite-Difference Time-Domain (FDTD) approach. These curves give the information about the path traversed by light and the power losses incurred in the waveguides.

Firstly, the 2D photonic directional coupler is presented based on a square lattice. The directional coupler is optimized for its performance as a 3dB coupler with minimum losses. By introducing the appropriate defects, the coupling strength of the coupler is increased and therefore, the coupling length required is reduced at the operating length. In the second work, we investigate the design of add drop filters on two dimensional square photonic crystal lattice. The filters are based upon multiple quasi-ring cavities inside the square cavity. They are designed to have perfect drop of desired wavelengths to the specified ports and to have high drop efficiency. Thirdly, the (1x2) wavelength router, also based on the square 2D photonic crystal lattice, is investigated for its efficient

performance. The conventional photonic waveguides of the order of lattice constant of the crystal structure are also introduced in this design for reducing the transmission losses. For all the above designed structures, the FDTD and PWE methods are implemented using OptiFDTD software, where these structures are analyzed critically from the obtained results.

TABLE OF CONTENTS

LIST OF FIGURES

LIST OF TABLES

LIST OF ABBREVATIONS

ADF	Add Drop Filter
BPF	Band Pass Filter
CMT	Coupled Mode Theory
CT	Crosstalk
CW	Continuous Wave
CWDM	Coarse Wavelength Division Multiplexing
DC	Directional coupler
EM	Electro-magnetic
FDTD	Finite Difference Time Domain
FSR	Free Spectral Range
LED	Light Emitting Diode
MZI	Mach-Zehnder interferometer
NDBP	Normalized Delay-Bandwidth Product
PBG	Photonic Band Gap
PC	Photonic Crystal
PCRR	Photonic Crystal Ring Resonator
PhC	Photonic Crystal
PhCDC	Photonic Crystal Directional Coupler
PWE	Plane Wave Expansion
Q FACTOR	Quality Factor
SIM	Strong Inverse Method

SOI	Silicon on Insulator
TE	Transverse Electric
TM	Transverse Magnetic
VCSEL	Vertical Cavity Surface Emitting Laser
WDM	Wavelength division Multiplexing

1.1 INTRODUCTION

Evolution of the photonic crystals is marked by the fact that rather than using high refractive indexed materials to trap and guide light waves, the photonic crystals known for the complete repulsion of light can be used as efficient guiding structures. Optical waveguides are formed by removing the material of the photonic crystals in a line, which creates the channels through which propagation of light is possible. In photonic crystals light can be guided through the low index materials, even vacuum and can easily turn through the sharp bends [1]. Photonic crystals have a different operational mechanism, thus they offer new opportunities for ultra compact devices and other nano-structures [2].

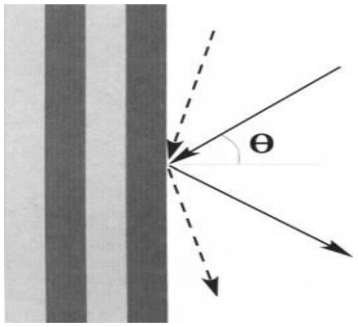

Figure 1.1 A simple 1D multilayer photonic crystal [2]

The photonic crystals are periodic dielectric structures which compose of alternate high and low refractive index materials. The refractive index repeats after certain period which is of the order of the wavelength of light. The photonic crystal can have these periodic variations in one, two or three dimensions, which makes them resemble various solid state crystalline materials. This is the main reason that due to their periodic alignment, they are called “crystals”. So, when light incident on the photonic crystal travels through the periodic structure, it experiences the reflection at each interface between the two alternative refractive indices as it travels by. Therefore, these multiple reflections interfere constructively and destructively with one another. In addition, if period of the crystal structure is made comparable to half wavelength i.e. $\lambda/2$ of the light incident, these reflections dominates the optical behaviour of the material. The spectral range of frequencies is there, centred at $\upsilon = c/\lambda > 0$ (where υ is the frequency, c is velocity of light

in vacuum), known as photonic band-gap (PBG) [1], in which propagation of light is forbidden as it is totally reflected.

1.2 HISTORICAL EVOLUTION OF PHOTONIC CRYSTALS

The photonic crystals are the main topic of study in one domain or the other since 1887. The "photonic crystal" term was first coined much later than its discovery in 1987. Before 1987, the photonic crystals were known as the periodic layers of the dielectric stacks in the researches, for example, the Bragg mirrors. In 1887, Lord Rayleigh had begun their research with the demonstration of the structures having a band of forbidden frequencies in a dielectric structure, also known as photonic band gap. It is a range of frequencies experiencing the high reflections analogous to a stop-band. Nowadays, photonic crystal structures are widely used in numerous applications whether the LED reflective coatings for their efficient working, or the mirrors with high reflection coefficient used in the laser, e.g. VCSEL. A comprehensive detailed research of stacked 1D multilayered photonic structure was carried out by Vladimir P. Bykov [3], and he was foremost to discover that the atoms and molecules in a photonic crystal emits spontaneously which is affected by the photonic band gap. Bykov studied the two and three dimensional periodic photonic crystals also. Then after Bykov, Ohtaka was the one to discuss the 3D photonic crystal in the year 1979 [4], who mathematically formulized his study for calculating the photonic band gap possessed by the crystal. But his ideas were not acknowledged till the time Yablonovitch and John [5, 6] had published their research work in 1987. They rigorously studied about the higher dimensional photonic crystals in their work. After them, the research on photonic crystals grew exponentially and many papers got published. But, because of difficulty in fabrication of the photonic crystal structures at nano scales, the early studies remain on papers or were fabricated in the microwave region, because these structures can be easily embedded on the centimetre scale. It was possible because electromagnetic fields possess a property of scale invariance, i.e. the solutions to Maxwell equations, i.e. E and H fields have no default scale, and therefore the centimetre scale at the microwave frequencies can be placed for the nanometre scale at optical frequency range. Yablonovitch calculated the first 3D photonic band-gap in the microwave range of frequencies in 1991. Yablonvitch had designed a structure having an array of holes drilled in a glass like substrate, where holes in each layer are forming an inverse diamond structure, called Yablonvitch nowadays.

Techniques using photonic slabs include the 2D photonic crystals etched into the dielectric slabs. The confinement of light in the 2D slab and photonic crystals is due to the total internal reflection similar to the effects of photonic dispersion observed in the slabs. Scientists are still working all over the world for commercializing the photonic crystal slabs by using them in the integrated chips circuits and evolve the optical communications on the nano-chip devices.

The techniques studied however are far to enter into the commercial market. The two-dimensional photonic crystals are the first photonic crystals to enter the market with the introduction of photonic crystal fibres [7] (also known as holey fibres, due to the air holes running through them).

Table 1.1 Historical developments of Photonic Crystals

1987	EliYablonovitch and Sajeev John have published two landmark papers on the photonic crystals.
1991	Yablonovitch was a pioneer who studied the 3D photonic band-gap in the microwave region of frequencies.
1996	In this year, Thomas Krauss demonstrated a 2D photonic crystal at the optical wavelengths for the first time. [8]
1998	Philip Russell was pioneer to develop the photonic crystal fibres, for the purpose of having improved properties over the conventional optical fibres.
2000	An "inverse opal" device with a complete photonic band gap was presented at University of Toronto [9]
2006	Scientists discovered the naturally occurring photonic crystal in the Brazilian beetle scales.

The study of three-dimensional photonic crystals has progressed very slowly compared to their two-dimensional counterparts because of the high difficulties in the fabrication. It took three more years after Yablonovitch, however, before a specific dielectric structure was correctly predicted to have a complete band gap in three dimensions, by Ho et al.

[10]. Subsequently, a large number of systems with band gaps have been proposed based on theoretical calculations, and in many cases these structures have been fabricated and characterized at wavelengths ranging from the microwave regime to the infrared regime.

1.3 ELECTRO-MAGNETIC BASICS

To study the propagation of light in any photonic crystal requires the knowledge of the Maxwell equations. The basics of electromagnetic waves are discussed below in the following sections.

1.3.1 MACROSCOPIC MAXWELL EQUATIONS

All of macroscopic electromagnetism involving the flow of light is well-explained by the macroscopic Maxwell equations. They are (in SI units) [11],

$$\nabla . B = 0 \tag{1.1}$$

$$\nabla \times E + \frac{\partial B}{\partial t} = 0 \tag{1.2}$$

$$\nabla . D = \rho \tag{1.3}$$

$$\nabla \times H + \frac{\partial D}{\partial t} = J \tag{1.4}$$

Where 'E' and 'H' are the macroscopic electric and magnetic fields respectively, and D and B are the displacement and magnetic induction fields. ρ and J are the free charge and current densities respectively.

Next we define a relationship of D with E and B with H through the building relations for the case, we are dealing with. The components D_i of the displacement field D can be defined in the terms of components E_i of the electric field E via power series as given below [12]:

$$\frac{D_i}{\varepsilon_0} = \sum \varepsilon_{ij} E_j + \sum \chi_{ijk} E_j E_k + O(E^3) \tag{1.5}$$

Where $\varepsilon_0 \approx 8.854 \times 10^{-12}$Farad/m is the free space permittivity. In case of number of dielectric materials, it is appropriate to consider the given approximations. Firstly, assume that the field strengths are small enough to consider them in the linear regime and χ_{ijk} and therefore neglect the higher-order terms. Secondly, consider those macroscopic and isotropic materials, such that E(r, ω) and D(r, ω) are related by ε_0 times a scalar dielectric

function ε(r, ω), which is known as relative permittivity. Thirdly, neglect any explicit frequency dependence of the dielectric constant. Rather, select the material of the dielectric constant which is highly suitable to the bandwidth of the considered physical system. Lastly, focus primarily on transparent materials, having ε(r) to be purely real positive number.

Taking all these four assumptions to be satisfied, it can be written,

$$D(r) = \varepsilon_0 \varepsilon(r) E(r) \tag{1.6}$$

Similarly to equation (1.6), we have

$$B(r) = \mu_0 \mu(r) H(r) \tag{1.7}$$

(where $\mu_0 = 4\pi \times 10^{-7}$ Henry/m is the vacuum permeability), but for most of the dielectric materials, relative magnetic permeability μ(r) is approximately unity and thus it can be written,

$$B = \mu_0 H \tag{1.8}$$

Considering all of the factors to be in place, the Maxwell equations can now written as,

$$\nabla . H(r,t) = 0 \tag{1.9}$$

$$\nabla \times E(r,t) + \frac{\mu_0 \partial H(r,t)}{\partial t} = 0 \tag{1.10}$$

$$\nabla . [\varepsilon(r) E(r,t)] = 0 \tag{1.11}$$

$$\nabla \times H(r,t) - \frac{\varepsilon_0 \varepsilon(r) \partial E(r,t)}{\partial t} = 0 \tag{1.12}$$

In general, both electric field and magnetic field are complex functions of time and space. However the equations above are linear, so segregate the time dependence part from the spatial dependence, expanding the fields into a set of harmonic modes.

To easy the mathematical calculations use a generic hoax of having a complex field and consider the real portion of the equation for obtaining the physical fields. It simplifies the problem and we can easily write harmonic modes as a spatial pattern multiplied by a complex exponent value [1]:

$$H(r,t) = H(r) e^{-j\omega t} \tag{1.13}$$

$$E(r,t) = E(r)e^{-j\omega t} \tag{1.14}$$

For finding the equations that define the mode profiles at a particular frequency, substitute the above equations into (1.9) to (1.12) [1].

$$\nabla . H(r) = 0 \tag{1.15}$$

$$\nabla . [\varepsilon(r)E(r)] = 0 \tag{1.16}$$

The two divergence equations define the conditions having a straightforward physical interpretation: no point sources or sinks of displacement and magnetic fields are present in the medium. Equivalently, these fields constitute of the transverse electromagnetic waves. It can be explained as, if we have a plane wave

$$H(r) = a.\exp(ikr) \tag{1.17}$$

, for any given wave vector k, equation (1.15) and equation (1.16) require that $a \times k = 0$. The two curl equations define E(r) and H(r) as:

$$\nabla \times E(r) - j\omega\mu_0 H(r) = 0 \tag{1.18}$$

$$\nabla \times H(r) + j\omega\varepsilon_0\varepsilon(r)E(r) = 0 \tag{1.19}$$

Now, split the above equations. Divide the bottom equation of (1.6) by ε(r), and calculate the curl after division. Now substitute the first equation to eliminate E(r). Even, the constants ε_0 and μ_0 can be vanished to yield the speed of light in vacuum i.e.$c = 1/\sqrt{\varepsilon_0\mu_0}$. The result is an equation completely in terms of H(r) [1]:

$$\nabla \times \left(\frac{1}{\varepsilon(r)}\right) \nabla \times H(r) = \left(\frac{\omega}{c}\right)^2 H(r) \tag{1.20}$$

This is the master equation.

1.3.2 ELECTRO-MAGNETISM AS AN EIGEN VALUE PROBLEM

As discussed in the above sections, the heart of the Maxwell equations for a harmonic mode in a multiple dielectric medium is a differential equation for H(r), given by equation (1.20). The equation is elaborated as: a series and of operations are performed on a function H(r), if H(r) proves to be an allowable electromagnetic mode, the result is a

constant multiplied with the original function H(r). This situation is called an eigen value problem. If the result of an operation on a function is the function itself, multiplied by some constant, then the function is called an eigen function or eigenvector of that operator, and that multiplicative constant value is called the eigen value.

In this case, we categorize the left hand side of the master equation as operator Θ acting on H(r) like a traditional eigen value problem:

$$\vartheta\, \mathrm{H(r)} = \left(\frac{\omega}{c}\right)^2 H(r) \tag{1.21}$$

The eigenvectors H(r) are the spatial patterns of the harmonic modes, and the eigen values $(\omega/c)\text{^}2$ are proportional to the square of frequencies of those modes.

1.3.3 BLOCH WAVES AND BRILLOUIN ZONES

A photonic crystal relates to a periodic dielectric function $\varepsilon(\vec{x}) = \varepsilon(\vec{x} + \overrightarrow{R_\iota})$ in case of the primitive lattice vectors $\overrightarrow{R_\iota}$ (i = 1, 2, 3 for a crystal periodic in all three dimensions). the Bloch-Floquet theorem can be stated as: the solutions to Eq. 1.20 must be of the form $\vec{H}(\vec{x}) = e^{i\vec{k}\vec{x}}\vec{H}_{n,\vec{k}}(\vec{x})$ having eigen values $\omega_n(\vec{k})$, where $\vec{H}_{n,\vec{k}}$ is a periodic envelope function satisfying [13]:

$$\left(\overrightarrow{\nabla} + i\vec{k}\right) \times \frac{(\overrightarrow{\nabla} + i\vec{k})}{\varepsilon} \times \overrightarrow{H_{n,\vec{k}}} = \left(\frac{\omega(\vec{k})}{c}\right)^2 \overrightarrow{H_{n,\vec{k}}} \tag{1.22}$$

, which yields a different Hermitian eigen problem for the primitive cell of the lattice at each Bloch wave vector k. This primitive cell is a finite domain for the periodic lattice structure in all directions, defined by discretized eigen values labeled by n equals to 1, 2,... These eigen values $\omega_n(k)$ are the continuous functions of wave vector (k) which forms discretized "bands" on plotting them against k, also known as a band diagram or dispersion structure. Moreover, these eigen solutions are also periodic functions of wave vector, i.e. the solution at the wave vector k is the similar to the solution of wave vector k $+G_j$, where G_j is a primitive reciprocal lattice vector calculated as: $\overrightarrow{R_\iota}.\overrightarrow{G_J} = 2\pi\delta_{i,j}$. Hence, we compute the eigen solutions for k that lies in the domain of the primitive reciprocal lattice cell or the set of non-equivalent wave vectors nearest to the k = 0 (origin), where this set is known as first Brillouin zone.

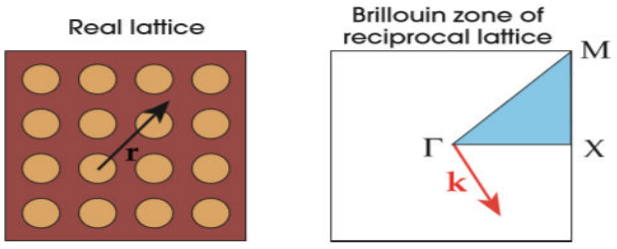

(a) (b)

Figure 1.2(a) A square lattice photonic crystal. An arbitrary distance vector r is marked. **(b)** The Brillouin zone of the square lattice with the origin (Γ). An arbitrary wave vector k is marked. Blue triangle wedge is irreducible region [1].

1.4 PHOTONIC CRYSTAL BASICS

We discuss the photonic crystals by taking the simplest case, i.e. one-dimension system. The electromagnetism principles and symmetry are applied to all the cases as discussed in the section 1.3. Even in the single dimensional system, we discern the most important parameters of a photonic crystal, such as photonic band gaps and localized modes around the introduced defects. We may be familiar with the optical properties of a one-dimensional photonic crystal, but the band structure and band gap calculation provide more insight into the behavior of the structure. We also discover new phenomena such as omni-directional reflectivity. Therefore, study of a single dimensional photonic crystal prepares us for the complicated two dimensional systems that lie ahead. Three dimensional photonic crystals are not introduced commercially because of the fabrication limitations. Thus we are not studying them in detail.

1.4.1 1D-PHOTONIC CRYSTALS

The simplest possible photonic crystal is one dimensional as given in the figure 1.3, consisting of multiple alternate layers of two dissimilar dielectric materials: a multi-layered film.

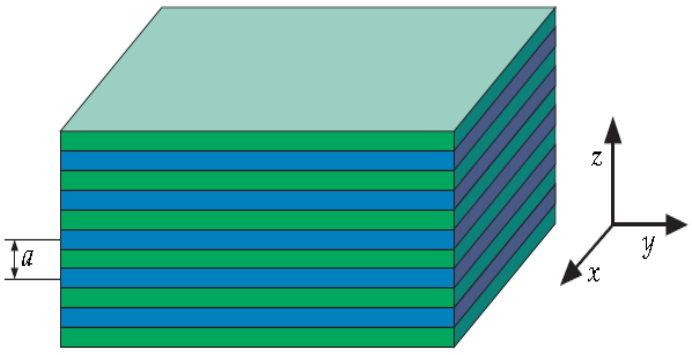

Figure 1.3 The multilayer film, a one-dimensional photonic crystal [1]

We describe the electromagnetic modes sustained by the crystal with the help of symmetry arguments. The dielectric material used in multilayered films has a well-defined periodicity in the z direction, and homogeneity in the x-y plane as there is no variation in this plane. We can therefore easily classify the modes considering the parameters, i.e. k_{ll} as the wave vector in the plane, k_z as the wave vector in the z direction,

and ‘n’ as the band number. The mode transformation is specified by the wave vectors by using the translation operators, and the band number indicates the band which increases with the frequency.

1.4.1.1 ONE DIMENSIONAL BLOCH STATES

For the one dimensional photonic crystal, the modes can be written in the Bloch Theorem’s form as follows:

$$\mathrm{H_{nkz}}(r) = e^{ik_z z}u(r) \tag{1.23}$$

The function u(z) is periodic, which is indicated by its property $u(z) = u(z + R)$, where ‘R’ is an integral multiple of the lattice constant ‘a’ in spatial co-ordinates. This photonic crystal is having a continuous translational symmetry in the x-y plane; therefore the wave vector k_{II} can assume any value. However, the wave vector in the z direction k_z is limited to a finite range, which is the 1D first Brillouin zone. It is because of the discretized translation symmetry of the crystal in the z direction having alternate refractive indices. When the primitive lattice vector is $\hat{a}_z$, the primitive reciprocal lattice vector is (2π/a) ˆz and the first Brillouin zone lies in the interval

$$-\frac{\pi}{a} < k_z \leq \frac{\pi}{a} \tag{1.24}$$

Because we know that k is repetitive outside the first Brillouin zone, the light line folds itself back into the first zone on reaching the edge. One can regard this as a way of relabeling the solutions of a Bloch theorem, in which (k + 2π/a) is replaced by k. The left most plot is for a homogeneous dielectric medium where we can arbitrarily assign a periodicity of ‘a’. But it is a general case of a homogeneous medium, where the velocity of light is decreased by the index of refraction. The modes lying with the light are given by the eqn. (1.25) [1],

$$\omega(k) = \frac{ck}{\sqrt{\varepsilon}} \tag{1.25}$$

The centre plot for a nearly-homogeneous medium is like the homogeneous case with the important distinction that a gap in frequency is there in between the upper and lower bands. There is no allowed mode of the frequency within this gap inside the crystal, regardless of k. This is the photonic band gap of the one-dimensional crystal structure. The rightmost plot has band gap widened because of higher contrast among the dielectric constants of the layers.

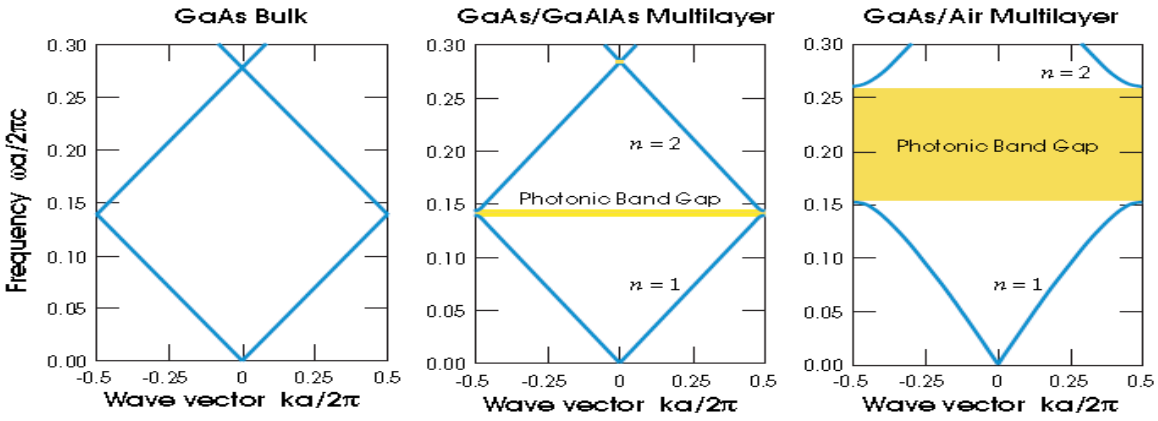

(a) (b) (c)

Figure 1.4 The photonic band gap structures for on-axis propagation, as computed for three distinct multilayered structures. In each case, single layer width is 0.5a. **(a)** Every layers is of similar dielectric constant ε=13. **(b)** Alternate layers of ε equals to 13 and 12. **(c)** Alternate layers of ε equals to 1 and 13[1].

The photonic band gap among the bands n = 1 and n = 2 happens to be at the edge of the first Brillouin zone i.e. $k = \pi/a$. We have observed that the lower frequency modes tends to localize their energy in the high dielectric regions, and the higher frequency modes have a most of their energy (although not necessarily a majority) in the low-ε regions.

1.4.2 2D-PHOTONIC CRYSTALS

The light propagation in the two dimensional plane has the harmonic modes categorized into two independent polarizations, with their own band structures respectively. We can introduce defects here, in order to localize the light modes, but we can localize a mode in two dimensions, rather than in just one dimension.

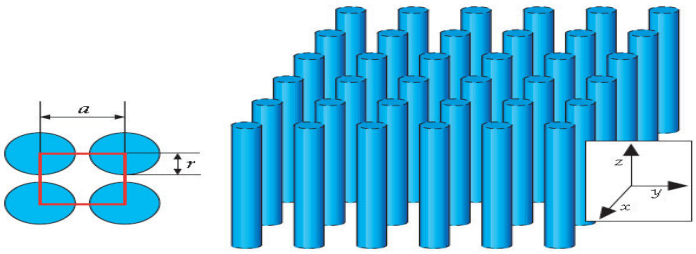

Figure 1.5 A 2-D Photonic Crystal [6]

1.4.2.1 TWO DIMENSIONAL BLOCH STATES

Unlike the multilayered film, the two-dimensional photonic crystals prevent light from travelling in any direction in the plane. The structure has homogeneity in the z direction, as a result of which the modes oscillate in that one direction only without any limitations

on the wave vector k_z. Also, the structure has discretized translation symmetry in the x-y direction.

The equation (1.26),

$$\varepsilon(r) = \varepsilon(r + R) \tag{1.26}$$

holds only if R is a linear combination of the primitive lattice vectors $\hat{a}_x$ and $\hat{a}_y$. The main dissimilarity is that in this problem, k_{II} is limited to the Brillouin zone and k_z is unbounded. In the multilayered 1D structure, the two wave vectors significance is contrast to each other as in this case. The photonic band structures for TE and TM modes are totally distinct. There can be a case when the photonic band gaps exist for one of the polarizations but not for the other. Let us consider a square lattice example in the next section.

1.4.2.2 SQUARE LATTICE OF DIELECTRIC COLUMNS

Consider light that propagates in the x-y plane of a square array of dielectric columns, such as the structure given in fig.1.5, with lattice constant 'a'. The band structure for a crystal of alumina ($\varepsilon = 8.9$) rods in air, having radius r/a = 0.2, shown in fig. 1.6. The horizontal axis depends on the value of the in-plane wave vector k_{II}. Wave vector k_{II} moves along the triangular edge of the first Brillouin zone, from Γ to X to M, from left to right as given in the left inset to fig. 1.6. We plot k_{II} traversing the edges of the Brillouin zone because the minima and the maxima of any band (which defines the band gaps) always happen to be at the zone edges, and in most of the cases at a corner. One should work with larger band gaps as much as possible, to maximize the mode localization.

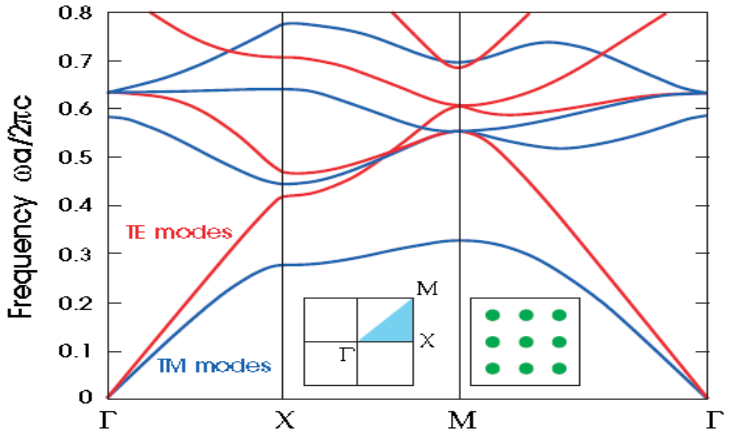

Figure 1.6 The photonic band gap for a square array of dielectric rods. The left inset has the irreducible Brillouin zone in light blue. The right inset has a cross-sectional view of the dielectric rods in a lattice. The rods (of ε=8.9 (alumina)) are rooted in the air wafer (ε=1) [1].

1.5 MATHEMATICAL TOOLS

Presently, the best way to study the optical properties of periodic lattice structures such as photonic crystals is the numerical methods. Plane wave expansion (PWE) and Finite-Difference Time-Domain (FDTD) are the most popular numerical methods used for calculating the band structure and extracting the PBG of photonic crystals. PWE method calculates the eigen frequencies and dispersion properties of photonic crystals, by numerically solving the Maxwell equations in frequency domain [1]. Calculating the accurate results and high speed are the most significant advantageous of PWE method [14].

1.5.1 FINITE DIFFERENCE TIME DOMAIN (FDTD) TECHNIQUE

The FDTD technique is the most used and simpler technique for calculating the solutions of Maxwell's equation splitting the structure into Yee's mesh [15]. The electric field 'E' and the magnetic field 'H' are computed at the grid points which are placed Δx, Δz distance apart. The time axis is also divided into the discrete points placed Δt apart. The E field is computed at time steps (n Δt) whereas the H field at time steps placed at the points $(n + 1/2)\ \Delta t$, while 'n' is the count of the computational iteration. The light signals that propagate in the photonic crystals, their behaviour and the penetration depth of their E and H fields can be efficiently studied using this method. This technique is a complete solution of Maxwell's equations without considering any approximations and limitations. In the 2D photonic crystals, split the fields into two transverse modes, i.e. E and H polarized modes. The Maxwell's equations are divided into discrete steps spatially and in the time domain with the help of Yee-cell method as discussed [15]. The FDTD time step formulae, i.e. the spatial and time division of Maxwell Equations on a discrete 2D mesh in the X-Y co-ordinate system for the E-Polarized mode are given below [15].

$$Ex(i,j,n+1) = Ex(i,j,n) + \frac{c\Delta t}{\varepsilon}\left[\frac{Hz\left(i,j+\frac{1}{2},n+\frac{1}{2}\right) - Hz\left(i,j-\frac{1}{2},n+\frac{1}{2}\right)}{\Delta y}\right] \tag{1.27}$$

$$Ey(i,j,n+1) = Ey(i,j,n) - \frac{c\Delta t}{\varepsilon}\left[\frac{Hz\left(i+\frac{1}{2},j,n+\frac{1}{2}\right) - Hz\left(i-\frac{1}{2},j,n+\frac{1}{2}\right)}{\Delta x}\right]$$

(1.28)

$$Hz\left(i,j,n+\frac{1}{2}\right) = Ez\left(i,j,n-\frac{1}{2}\right) + \frac{c\Delta t}{\mu}\left[\frac{Ex\left(i,j+\frac{1}{2},n\right)-Ex\left(i,j-\frac{1}{2},n\right)}{\Delta y}\right] - \frac{c\Delta t}{\mu}\left[\frac{Ey\left(i+\frac{1}{2},j,n\right)-Ey\left(i+\frac{1}{2},j,n\right)}{\Delta x}\right]$$

(1.29)

,while the index 'n' denotes the nth time step and 'i' and 'j' are the spatial grid points in the X-Y plane. The FDTD method solves the given equations iteratively calculating the E and H fields at their respective time steps alternately.

The time monitor (detector) is placed in the photonic channels for calculating the electric field that varies with time. It records the power through the channel as a function of time. The total power at the output is the integrated power of the individual cell as shown in equation (1.30) given below. The result obtained is hence Fourier transformed and integrated. The output signal power is

$$P(t) = \frac{Re\left[\int_A [E(t)\times H^*(t)]dA\right]}{Re\left[\int_A [E(t_o)\times H^*(t_o)]dA\right]} \quad (1.30)$$

, where 'A' is the plane in the waveguide section where time monitor is placed. The length of the time monitor has no role as power is integrated over the plane lying in X and Z axis [16].

1.5.2 PLANE WAVE EXPANSION (PWE) METHOD

To calculate the photonic band gap and find the propagating modes of the photonic crystal, the plane wave expansion method is implemented in most of the cases. This method gives the band gap structure to observe various bands and the gap between them. Band gap can be calculated for both transverse electric and transverse magnetic polarizations. The periodic photonic crystal structure composed of dielectric rods is expanded in the Fourier series. The band gap structure calculated by this method is a region in the first Brillouin zone. The X-axis has the values obtained by connecting Γ-X-

M-Γ points in k-space as shown in the left inset of the fig. 1.6 and Z-axis is the normalized frequency (ωa/2πc = a/λ) of either TM polarized wave or TE polarized light wave mode that propagates in the simulated structure. The band diagram generated is actually the solution to the master eqn. 1.20. This equation as explained earlier is a result of Bloch-Floquet theorem which describes the propagation of light in photonic crystals and signifies that this propagation can be without scattering, governed by the periodic function with period of a lattice modulated by a plane wave.

Because of the periodic 2D periodic photonic crystal, the dielectric constant, ε can be stated as [13],

$$\varepsilon(r) = \varepsilon(r + R) \tag{1.31}$$

where R is a 2D random lattice vector. The solutions of this eigen value periodic problem is given by Bolch-Floquet theorem, written as

$$\vec{H}(\vec{x}) = e^{i\vec{k}\vec{x}}\vec{H}_{n,\vec{k}}(\vec{x}) \tag{1.32}$$

It has eigen values $\omega_n(\vec{k})$, and $\vec{H}_{n,\vec{k}}$ is a periodic envelope that satisfies [13]:

$$\left(\vec{\nabla} \times i\vec{k}\right) \times \frac{(\vec{\nabla}+i\vec{k})}{\varepsilon} \times \overrightarrow{H_{n,\vec{k}}} = \left(\frac{\omega(\vec{k})}{c}\right)^2 \overrightarrow{H_{n,\vec{k}}} \tag{1.33}$$

For any Bloch wave vector k, the eigen equation (1.32) divides itself on the basis of a plane wave for yielding an algebraic eigen value problem which are easily solved at the permissible values of frequencies ω of the modes characterized by the eigenvectors. If we scan the wave vector k over the first Brillouin zone, the band diagram is generated.

1.6 OPTIFDTD SOFTWARE

All the above techniques, FDTD and PWE are applied on the photonic crystal designs by carrying out their simulations using OptiFDTD software [16].

About the software OPTIFDTD:

OptiFDTD has 4 main applications:

1. Layout Designer: The photonic crystal design must be defined within it. The different simulation conditions are also specified in this domain.

2. Profile Designer: This module is used for defining different materials and profiles which are used in designing the circuit for simulation.
3. Simulator: This programming module is used for loading the designed file and to perform the simulations. The beginning module is the designer module as complete layout is specified there.
4. Analyzer: This programming module is for viewing the simulation results and for performing any post simulation analysis. The moment, the simulation is completed; user is asked if he would like to have the analyzer window opened.

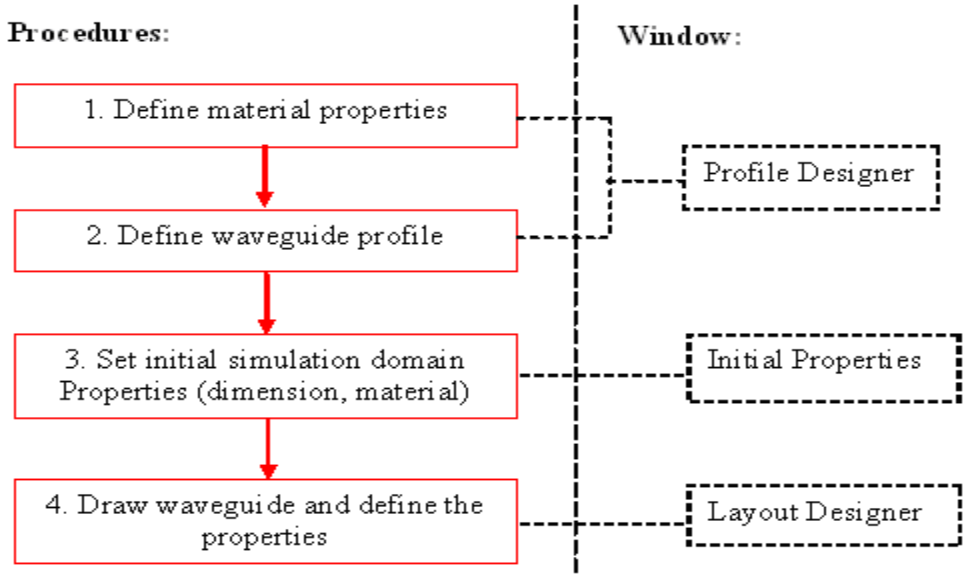

Figure 1.7 Flow chart for building a Layout in OptiFDTD [16].

1.7 ADVANTAGES OF PHOTONIC CRYSTALS

As we know, light has several advantages compared to the electrons. It travels in a dielectric at much higher speed than the electrons in a metallic circuit. Light carries huge amount of information in a second i.e. bandwidth of the optical fibers is of the order of terahertz whereas electronic systems has of few hundred kilohertz [17]. Also, light is far less interacting than electrons, thus reducing energy losses to a large extent.

Despite having several advantages, optical circuits have not yet ruled the commercial market. Designing a multipurpose optical component analogous to the electronic component such as transistors is very difficult because of the fabrication techniques, high confinement requirements, losses incurred at the bends and turns of the optical paths.

However, photonic crystals are the new hope for scientists. The idea of designing photonic crystals is that they can affect the properties of light in much similar way that semiconductor crystals affect the properties of electrons. Few advantages are listed below:

- High confinement of light:

  The devices based upon the photonic crystal has an advantage of better confinement of light as compared to their conventional counterparts as the photonic band gap possessed by the crystal does not allow the light to penetrate through the walls of the waveguides created.

- Low losses:

  The operating speeds and output efficiencies are not affected due to small sizes of the structures as the photonic crystal guides the light through the bends and turns easily due to high confinement property.

- Miniature Sizes:

  Because of the properties discussed above, miniature sized devices are possible having efficient performance.

- High packing density:

  Lesser the size of the components, more the number of components can be assembled on an integrated chip. Owing to the nanometer feature sizes of the photonic crystal structures, density can be increased.

Other significant properties possessed by the photonic components like filters, couplers etc. are their high spectral selectivity, fast switching capability and low power consumption.

1.8 LIMITATION OF PHOTONIC CRYSTALS

Although the photonic crystals have several advantages owing to their use in technology industry, they are still theoretical. The main limitation in the commercialization of the photonic crystals is the difficulty in fabrication [7].

Three dimensional photonic crystals are very hard to fabricate. The periodic variation in the dielectric constant on a three dimensional scale of the order of micrometers has to be precise and it demands very careful integration for photonic devices to work properly.

1.9 OBJECTIVE OF DISSERTATION

The objective of this dissertation is to design and analyze various two-dimensional photonic crystal devices and optimize the performance efficiencies by introducing appropriate defects in the crystal. The photonic band-gap for each structure is found with the help of Plane Wave Expansion method as discussed in the section 1.5.2. The power transmittances are calculated using FDTD approach which solves the Maxwell's light equations in an iterative form, discussed in section 1.5.1. In this dissertation, three fundamental guiding structures in the domain of optical communication are designed, which are directional couplers (DC), add/drop filters (ADF) and wavelength routers. The main objectives of this work are:

1. To improve the coupling strength of directional coupler based on 2D square photonic crystal lattice. More the coupling strength, shorter is the coupling length required for a DC and higher is the coupling coefficient. Therefore, the designed DC is to be optimized for its integration in the miniature sized circuits.
2. To attain high drop efficiency of an add/drop filter based on 2D photonic square crystal lattice by varying its design parameters. The trade-off between drop efficiency and spectral width is to be optimized in the design.
3. To achieve high power efficiency of the 2D photonic crystal wavelength router with the introduction of conventional waveguides in the photonic structures. To optimize the device to efficiently separate the wavelengths of 1.52 μm and 1.6 μm with minimal crosstalk and transmission losses.

1.10 ORGANIZATION OF DISSERTATION

In this chapter, we have already discussed all the basics required to understand the behaviour of light traversing in a photonic crystal and to solve the Maxwell's equations to mathematically analyze the problem. Rest of the work is organized as follows.

Chapter 2 discusses the literature survey done for the understanding of concepts of photonic crystals as well as to define the main objectives of the thesis. The works of different authors are studied comprehensively to know various techniques and methods to device a circuit and critically analyze it. And therefore, we find gaps in their works and aim at improving the circuits further.

Chapter 3 demonstrates 1x2 directional couplers (DC) on the 2D photonic crystals based upon the light coupling employing the evanescent field interaction. Two alternative 3-dB configurations of (1x2) asymmetric DC based on a square lattice are discussed. The coupling strength is measured in terms of the coupling length and coupling coefficient. The PWE and FDTD simulations are carried out using OptiFDTD software.

Chapter 4 investigates the design of add drop filters on two dimensional square photonic crystal lattice. The simulation set up and results are analyzed thoroughly for two alternative ADF layouts.

In chapter 5 we have designed the (1x2) T-shaped wavelength router based on 2D square photonic crystal lattice having Si rods embedded in air wafer. The conventional photonic waveguides of relatively lower refractive index ($Si0_2$) are introduced at various points in the photonic crystal waveguides (air). The FDTD and PWE simulations are carried out for analysis of the device.

Chapter 6 has the conclusion, recommendation and future scope of the work done.

CHAPTER 2

LITERATURE SURVEY

Photonic crystals (PhC) have acquired a great interest in them since the last decade and are considered good candidates for their use in various optical transmission systems. Owing to their unique properties, they have numerous advantages such as easy fabrication, better light confinement through the bends, low power consumption and miniature sizes etc. With the introduction of defects in the perfect photonic crystals, various PhC circuits have been realized efficiently. Many authors have done research on various optical components and have studied their behaviour in several aspects. The different parameters of the components are investigated and change in the outputs with change in the parameters in reported.

The literature survey by various authors in the past few years has been discussed below:

Zexuan Qiang et al. [2]

This work demonstrates the ultra compact photonic crystal add/drop filter based on ring resonators. The finite difference time domain method has been used to calculate normalized power for both single resonator and two resonators structures on a square lattice. Moreover, authors have designed the structure for good selectivity and 100 % dropping efficiency with the help of scatter rods in the sharp corners of the ring. The structure controls the drop efficiency in both backward and forward drop for different resonant modes symmetries. Authors also analyzed the tunability of the structure with the change in wavelength and compared the Q-factor. More than 96 % drop efficiency is obtainable having Q-factor in the range of 160 to 10^3.

A. Ghafari et al. [19]

The add/drop filter discussed in this work is the main component of the optical add/drop mux, photonic modulation circuits and switches. This filter is also designed based upon the ring resonators owing to the higher Q-factors and ring's single mode nature. Authors have analyzed the frequency response and the coupling characteristics of the structure. They have also added the scatterer rods at the corners of the rings and thus have analyzed the effect of change of radii of coupling and scatter rods on the resonating wavelength shifts. Even dielectric of the inner rods has been varied for tunability.

Ahmed Taalbi et al. [20]

Authors have presented a novel design of channel add/drop filters (CDF) on a triangular 2D photonic crystals lattice. This CDF is also based upon the ring resonators and is investigated using the finite difference time domain (FDTD) method. This CDF has achieved the backward drop with efficiency of 96% and forward drop having efficiency up to 98% in the third communication window. The effect of change of radius of coupling rods and change in dielectric of the structure on the resonant modes is also studied in this work.

P. Andalib et al. [21]

The authors have discussed a novel design of add/drop filter which is based on the 2D photonic crystal ring resonators. It finds its application in ultea compact devices and circuits owing to its small size. The structure is analyzed using FDTD approach and plane wave expansion (PWE) method solves the band gap. The add/drop filters are mainly used in wavelength division multiplexing (WDM) systems.

Weidong Zhou et al. [22]

An add/drop filter based on 2D photonic crystal ring resonators (PCRR) are reported in this research work. This ADF works as both backward dropping and forward dropping filter with two different mode symmetries. Tunability with the change in parameters and the scalability of the circuit is also analyzed in this paper for the multiplexers and photonic switches.

J. Romero Vivas et al. [23]

Authors have studied the octagonal quasi periodic structure based on the 2D photonic crystals. The photonic band gap is analyzed with the help of PWE method. TM polarization finds a complete band-gap with the dielectric constant as low as 1.6. The micro-cavities and waveguides are also studied for their properties to design an add/drop filter. And authors have also presented an add/drop filter structure optimized for its good performance. The FDTD method is used for the numerical analysis of the structure.

S. Robinson et al. [24]

This work presents an add/drop filter based on the 2D photonic crystal ring resonator to work with ITU-T G.694.2 Coarse Wavelength Division Multiplexing (CWDM) systems to add/drop a channel at a resonant wavelength of 1491 nm. The transmission spectra of the structure and band gap are calculated using FDTD and PWE method respectively.

Dropping efficiency of 100 % is obtained with the spectral width of 13 nm and Q factor is 114.69 at the 1491 nm. For resonance tuning with the wavelength, change in various parameters such as lattice constant and radius of the lattice rod is analyzed.

M. Djavid et al. [25]

In this research work, multi-channel drop filter is proposed based upon the 2D square photonic crystal ring resonators (PCRR). Transmittance spectrum is investigated numerically using the FDTD method. This multi-channel drop filter is designed with three waveguides and ring resonators in two separate regions with different dielectric constant. The input power at resonant wavelength deviates to one of the three waveguide exit ports and output efficiency is more than 81%.

Mahmoud Youcef Mahmouda et al. [26]

In this research, the photonic add/drop filter based on 2D PCRR is proposed. The filter is designed in two-dimensional photonic crystals triangular lattice. The FDTD method is used for analysis of the drop efficiency where forward efficiency is 100% at 1550 nm. The effects of change in various parameters such as the dielectric constant and radii of both whole rods and coupling rods are investigated. This 10.9 μm × 10.3 μm sized structure is suitable for integration in the circuits.

Rajib Ahmed et al. [27]

Here, authors have discussed the ultra compact power splitters with 1x2, 1x4 and 1x6 channels with T-junction, Y-junction and multiple line defects respectively. The structure is integrated with multiple mode interfering blocks. The proposed structure is simulated using FDTD approach. This paper aims at optimizing various parameters like rod radius, input diameter, resonant wavelength and the substrate refractive index. 1 × 2 for Y-Junction shows maximum power transmission.

Justin Stewart et al. [28]

Here the authors have proposed a design of a micro flow cytometry based on photonic crystals. The light transmission changes through the photonic crystal depending on whether a cell is present or absent and shape and size while flowing tangential to the surface. The design is simulated using FDTD approach on the optiFDTD software. This design significantly shows a variation in cell shapes analyzing the signal distributions.

S. Dominguez et al. [29]

Authors have presented the 2D photonic crystal onto silicon wafer for improving the performance of Si Photo-Voltaic cells. The main purpose of this work is to design a structure that can minimize the reflectance of the Si wafer.

Giovanna Calo et al.[30]

Here authors have proposed an optical 1x2 passive wavelength router, based on 2D PCRR. The behaviour of a 4x4 router design by merging eight 1x2 routers on a single circuit is investigated for the minimum crosstalk. The design criteria are pointed out, and the spectra and band gap results are calculated using FDTD approach and PWE method respectively.

S. Robinson, et al. [31]

In this research, the bandpass filter (BPF) is designed based on 2D PCRR that works for the range of C and L+U bands in CWDM devices. The structure consists of two quasi waveguides and one ring resonator; and the transmission spectra and photonic band gap is calculated using FDTD approach and PWE respectively. The BPF1 works between 1530 to 1565 nm in the C-band and BPF2 at 1565 to 1675 nm in L+U bands (BPF2). The size of the structure is of the order of micrometers i.e. BPF1 is 12.8 μm × 11.4 μm and 11.4 μm × 11.4 μm for BPF2.

Kiazand Fasihi et al. [32]

In this work, the waveguide intersection based upon two photonic crystal (2D square lattice) hybrid waveguides orthogonal to each other is presented. The transmission results are formulated using FDTD and coupled-mode theory (CMT) methods. The bandwidth (BW) and crosstalk of the hybrid structure are calculated for different radii of the coupled cavities. The intersection is shown to have negligible crosstalk with negligible interference and low distortion between the light signals crossing through it.

Guimin Lin et al. [33]

In this research, the new design of 1 × 4 optical multiplexer based on 2D photonic crystal is presented which has the cascaded Mach-Zehnder interferometer (MZI) embedded in it, responsible for the self-collimation effect. This structure has four beam splitters and five mirrors in it. The numerical transmission spectra at various output ports are calculated with the light interference theory and thus simulated using FDTD to verify the results. The results indicated the cascaded MZI can work as a 1 × 4 multiplexer with the

appropriate path length. At the wavelength 1550 nm, the free spectral range (FSR) is 24 nm in the C-band window. This device has compact size and high output efficiency.

Wei-Yu Chiu et al. [34]

In this paper, the ring resonator filter based on a hexagonal photonic crystal (silicon on insulator) is demonstrated. This PCRR simultaneously separates the light at wavelengths of 1.31 and 1.55μm. Fabrication of this device is carried out by e-beam lithography. The results confirm the 1.31μm/1.55μm wavelength ring resonator with nano-silicon rods on a insulated wafer can be realized.

Kao-Der Chang et al. [35]

In this paper, the electro-optic switch based on photonic crystal waveguide and cavity coupled sideways is reported. The coupling between the twin cavities and the line waveguides is investigated with the Maxwell's equations solutions. The basic characteristics of the coupling structure are studied to have efficient drop tunnelling. Electrical tunability of the resonant modes is observed by modulating the cavities conductance.

Junjie Bao et al. [36]

Authors have investigated a new design of all-optical logic gates based on 2D square lattice photonic crystals. The proposed device has a cross-shaped waveguide and two PCRRs without non linear materials and amplifiers. The logic gates design simulation is carried out by FDTD method and band gap is calculated by using PWE technique. These optical logic gates are observed to behave as NOR and NAND logic gates and has much potential to be used in large-scale logic integrated circuits.

W. Y. Chiu, et al. [37]

In this paper, authors have demonstrated the use of photonic crystal (PC) directional couplers to separate light of wavelengths at 1.31 and 1.55 m. The PC structure consists of InAlGaAs nano rods arranged in hexagonal lattice. The device is simulated using FDTD approach and is thus fabricated by e-beam and conventional photolithography. The design pattern is smoothened with the application of strong inverse method (SIM) of e-beam lithography. The experimental results verify the separation of 1.31/1.55μm wavelengths, with the PC structures formed.

Solomon Assefa et al. [38]

In this paper, authors have designed and fabricated the photonic crystal structure composed of the combination of the high refractive-index GaAs/AlxOy material system fabricated with electron-beam lithography at 1.5 μm wavelength of light. The transmission spectra were obtained for structures consisting of a 2D array of rods and line-defect waveguides. Optical calculations confirmed the band gap present, and also the guided band gaps in the straight waveguide. A two-stage coupling facilitates the efficient coupling into that waveguide.

Na Zhu et al. [39]

In this work, authors have presented non linear coupled-cavity based on the non linear photonic crystal. Non linear photonic crystals are formed by introducing the Kerr effect non-linear rods into the perfect photonic crystal. The slow light properties and band gaps are studied with the help of PWE method. Authors have proposed both coupled cavity with a single defect and with dual defects for optimization of the slow light properties. The results obtained show that the single-defect cavity in a waveguide can obtain the larger Normalized Delay-Bandwidth Product (NDBP) but it cannot decrease the group velocity of light to a desired value, and thus cannot have good Q-factor. Whereas the two-defect cavity in waveguide reduces the group velocity of light efficiently and gives good Q factor.

A. Wirth Lima Jr. et al. [40]

Authors have designed and investigated the directional coupler based on a triangular lattice graphene photonic crystal that can work as a switch. The structure is designed on a SOI photonic crystal slab. The directional coupler has two straight waveguides and the coating of the coupling region is done with graphene ribbon having width of 50nm. Authors have used an electric gate for the modification of the chemical potential to result in change in graphene equivalent permittivity. Therefore, the designed directional coupler can easily transit from the bar state to the cross state and vice-versa.

Elyar Pourali et al. [41]

In this paper, authors have demonstrated the 2D triangular lattice silicon carbide based photonic crystal straight waveguides (SiC-PhC) with slow light capabilities. The crystal is simulated by embedding the air-hole in SiC substrate having an oscillator type refractive index. It is observed from the simulation results that by doing fluidic infiltration

selectively and variation in the air-holes radii, this structure can slow light down by the factor 473 approximately whereas their group velocity dispersions are nearly zero.

C. Sciancalepore et al. [42]

Here, authors have fabricated the vertical cavity surface emitting lasers (VCSELs) based on two sets of the photonic crystal mirrors that works at the long wavelengths. The main features of a device like modes, polarizations and thermal properties are extensively studied by the author. The results discussed have shown the flexibility of the photonic architecture designed. The light traversing through Si/SiO2 photonic crystals accounts for a tailored mode selection and full polarization control.

CHAPTER 3
DESIGN AND ANALYSIS OF 3-DB PHOTONIC CRYSTAL DIRECTIONAL COUPLERS

The 1x2 directional couplers (DC) on the 2D photonic crystals are devised based upon the light coupling employing the evanescent field interaction. The theoretical power transmittance spectra are analyzed using Finite-Difference Time-Domain (FDTD) approach for two alternative DC layouts. The simulation results indicate that the DC can work as a 3-dB coupler efficiently with the introduction of appropriate defects in the schematic. For the operational wavelength of 1467.1 nm, the coupling coefficient of DC is 0.057 (in the units of propagation constant) and the coupling length is 109 μm. Spectral bandwidth of the structure is 37.5 nm ranging from 1448 nm to 1485.5 nm in the S- Band window of WDM systems. This device finds its application in ultra-compact photonic circuits requiring high transmission efficiency as calculated reflection losses are less than 6% of the total input power.

3.1 INTRODUCTION

Photonic crystals (PhC) [6], [1] have acquired a great interest in them since the last decade and are considered good candidates for their use in various optical transmission systems. Owing to their unique properties, they have numerous advantages such as easy fabrication, better light confinement through the bends, low power consumption and miniature sizes etc. With the introduction of defects in the perfect photonic crystals, various PhC circuits have been realized efficiently, such as multiplexers/demultiplexers [42], interleavers [43], filters [44] etc.

Directional Couplers (DC) are one of the fundamental guiding structures in the optical communication. Recently many PhCDCs are designed both theoretically and experimentally due to their substantially shorter coupling lengths, as compared to the conventional integrated couplers. Basically DCs are the two waveguides placed in the close proximity, in which light launched in the one waveguide couples with the other waveguide periodically along the coupling length.

F. Cuesto Soto et al. demonstrated a directional coupler on a hexagonal lattice having high indexed alumina rods in air [45]. Intermodal dispersion in the coupler was observed

experimentally. M. K. Moghaddam et al. investigated the PhC directional coupler having improved coupling characteristics and coupling length less than three times the lattice constant [46]. However, the coupling power efficiency of this structure is significantly low due to reflection losses at the hexagonal bends. Yameng Xu et al. presented an asymmetrical PhC directional coupler for injection of light into slow light slot waveguide [47]. This approach leads to very low insertion losses but the bandwidth ranges from 5-10 nm only.

In all the above researches, we observe a trade-off between the efficient coupling parameters and the power transmittance efficiency. The operational bandwidth of the structures is very low. In this chapter, two alternative 3-dB configurations of (1x2) asymmetric PhCDC based on a square lattice are discussed. The coupling strength is measured in terms of the coupling length and coupling coefficient. The cavity defects are introduced at the Y-bend of DC to channelize the light from the primary waveguide (having the input source) to the secondary waveguide (coupled with the primary waveguide). The designed coupler divides the input power equally to both the output ports and hence, it is called 3-dB directional coupler.

3.2 THEORY

Directional coupler (1x2) is an asymmetrical Y-shaped coupler consisting of the two closely placed waveguides. The working principle of DC is the splitting of light stream launched into one of the waveguides to both of them because of the evanescent field interaction [48]. The amount of power output to the primary waveguide is called throughput. The power coupled to the secondary waveguide, is known as coupled power.

The efficient coupling of waveguide requires minimal dispersion which is largely intramodal. Any input guided mode splits into the two supermodes because DCs have an intrinsic property to disperse the light into multiple modes [45]. These supermodes are known to have even and odd symmetries with respect to the plane equidistant to waveguide axis. Therefore, the mismatch between these supermodes gives rise to intramodal dispersion.

Although asymmetric PhC couplers do not support pure even or odd propagation modes, however localized modes in the circuit can be designated into the categories: even-like and odd-like, i.e. if only in mirror plane, the modes are purely TE or TM, we can say that even modes are TE-like and odd modes are TM-like [49]. From the bandgap curves, we

get a relationship between angular velocity ω and wave vector k. Group velocity of an electromagnetic wave can be calculated as [45]:

$$v_g = \partial\omega/\partial k, \tag{3.1}$$

An incident pulse has its energy distributed between two supermodes and the difference between the group-velocity of modes is the origin of intramodal dispersion.

Coupling strength of the directional couplers is calculated in terms of the coupling parameters: coupling coefficient and coupling length. Both odd and even supermodes must have the same propagation constant for maximum coupling to take place between the waveguides. From the propagation constants of even and odd modes, we calculate coupling coefficient κ [49], where

$$\kappa = |k_{even} - k_{odd}|/2 \tag{3.2}$$

Light travelling through waveguides keeps on migrating between the two of them periodically. Beat Length is defined as the period of transfer of light [49], i.e.

$$L_B = 2\pi/|k_{even} - k_{odd}| \tag{3.3}$$

Similarly, another parameter is coupling length, which is the required distance for energy migration to occur between the two waveguides [49],

$$L_C = \frac{\pi}{|k_{even} - k_{odd}|} = L_B/2 \tag{3.4}$$

Power transmittances are calculated using FDTD algorithm, with anisotropic domain and PML (perfectly matched layer) boundary conditions. Bandwidth and Q-factor can be calculated from the power transmittance curves. Range of wavelengths for which efficient coupling takes place and coupled power is above the reference power, is bandwidth of the structure. Q-factor can be calculated as $\lambda_r/\Delta\lambda$ (Resonant wavelength / Bandwidth) [50].

The performance of an optical coupler is calculated as the percentage of the power between the output ports by calculating the coupling ratio given as [51]:

$$Coupling\ Ratio = \frac{P_{coupled}}{P_{coupled} + P_{throughput}} \times 100\ \% \tag{3.5}$$

where $P_{throughput}$ is the power output of port A (waveguide A) and $P_{coupled}$ is the coupled power output of the port B (waveguide B).

The amount of power coupled can be controlled by varying the different parameters of the waveguides such as coupling length, introduction of ring cavities at the bends, radius of the rods constituting the waveguides. With the proper adjustments of these parameters, we can have the power input equally divided among the two waveguides, called 3-dB coupler [51].

$$Throughput\ Power\ Ratio(in\ db) = 10\ log \frac{P_{throughput}}{P_{coupled}+P_{throughput}} \qquad (3.6)$$

Also, the loss due to backward reflections can be calculated by having the observation point towards the other end of waveguide B (other than the output), and power calculated at this point is given as $P_{reflected}$.

3.3 SIMULATION SET UP

Directional coupler is designed on a 2D square lattice in X-Z plane. Silicon rods (18 x 21) having refractive index of 3.47 and a radius of 0.175 times the lattice constant (540 nm) are placed in an air wafer. Two waveguides are formed by removing a series of rods, creating line defects which results in one straight waveguide (A) and the other Y-ended waveguide (B). Operational wavelength considered for this structure is 1467.1 nm continuous Gaussian wave input.

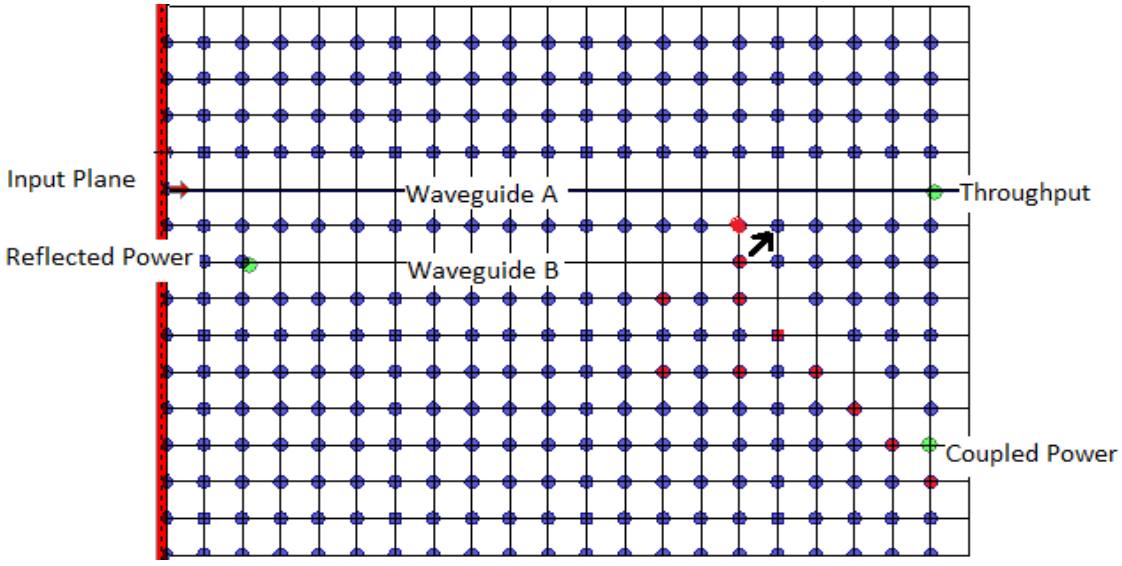

(a)

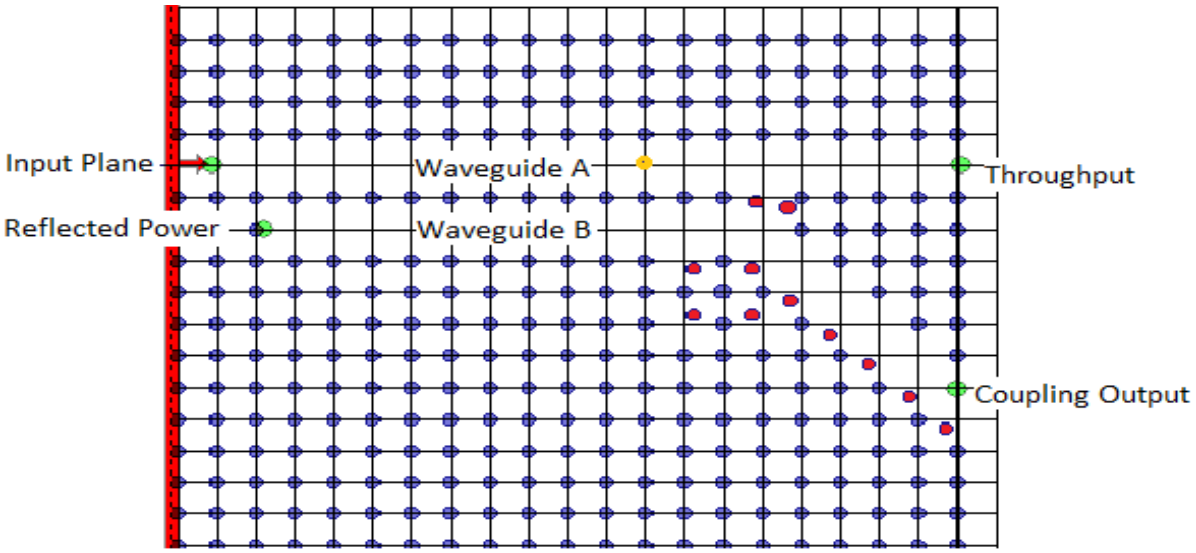

(b)

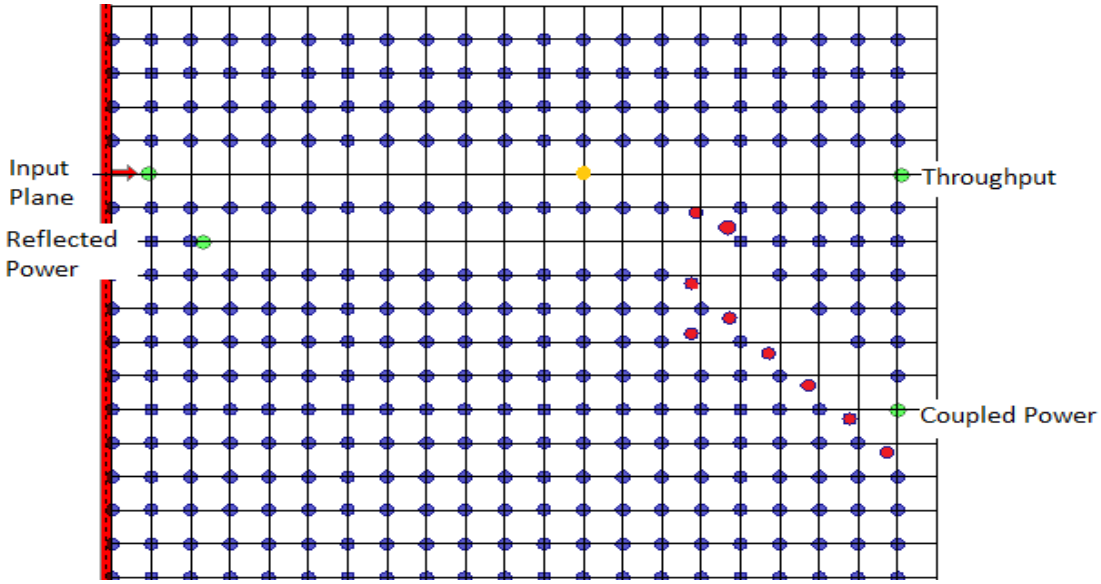

(c)

Figure 3.1 Schematic Layout of an asymmetrical Y-shaped directional coupler. The red arrowed vertical plane is the input plane. Three observation points (marked green) record the output powers at throughput port, coupled output port and reflected power. **(a)** Square Lattice structure with two waveguides is formed by removing the rods in a line (Line defects). No defects are introduced at bends. **(b)** All red marked rods at the bends and throughout the Y-crossing shown in fig. 3.1(a) are shifted from their original positions to form defects. Reflector rod in the primary waveguide A is introduced, shown in yellow. **(c)** Ring cavity defect at the Y-bend below waveguide B is modified to a semicircular ring defect.

All the silicon rods marked red are used for introducing defects. Along the Y-bend below the waveguide B, a first order ring resonating cavity is introduced as shown in fig. 3.1(b) to channelize the signal power through the Y-bend without losses. The sharp pointed edged red rods throughout the Y-crossing shown in fig. 3.1(a) are shifted inwards towards the lattice by the amount of one-fourth of lattice constant to minimize the reflection losses, as shown in fig. 3.1(b). The bend below the waveguide A is also modified by shifting rods to form an arc shape and the rod marked with a black arrow in fig. 3.1(a) is shifted upwards in the direction of arrow away from the centre of cell to smooth the upper bend. Rod in yellow shown in fig. 3.1(b), 3.1(c), is a reflector added to primary waveguide A to facilitate the coupling of power from the primary waveguide A to waveguide B and equalize the input power distribution between the two output ports. Without the reflector rod, most of the power channels through the throughout port, decreasing the coupling efficiency. In fig. 3.1(c) we observe that the Y-bend ring defect is modified to form the semicircular defect. This modification reduces the reflection power losses in waveguide B, improving the overall efficiency of the structure. We compare the configuration in fig. 3.1(c) to the configuration in fig. 3.1(b) numerically, as discussed in the section below.

3.4 RESULTS AND DISCUSSIONS

The DC structures given in fig. 3.1(b) and fig. 3.1(c) are simulated by launching the input Gaussian wave through the vertical input plane having wavelength of 1467.1 nm. At this wavelength, the circuits behave as a 3-dB coupler where the output ports of both waveguide A and waveguide B receive equal signal strength. Photonic Bandgap (PBG) simulations are performed using PWE method [52], where both TE and TM band gaps are calculated. TE bandgap for the defect free photonic crystal ranges from 1209 nm to 1783 nm whereas TM mode has no band gap as shown in fig. 3.2 below.

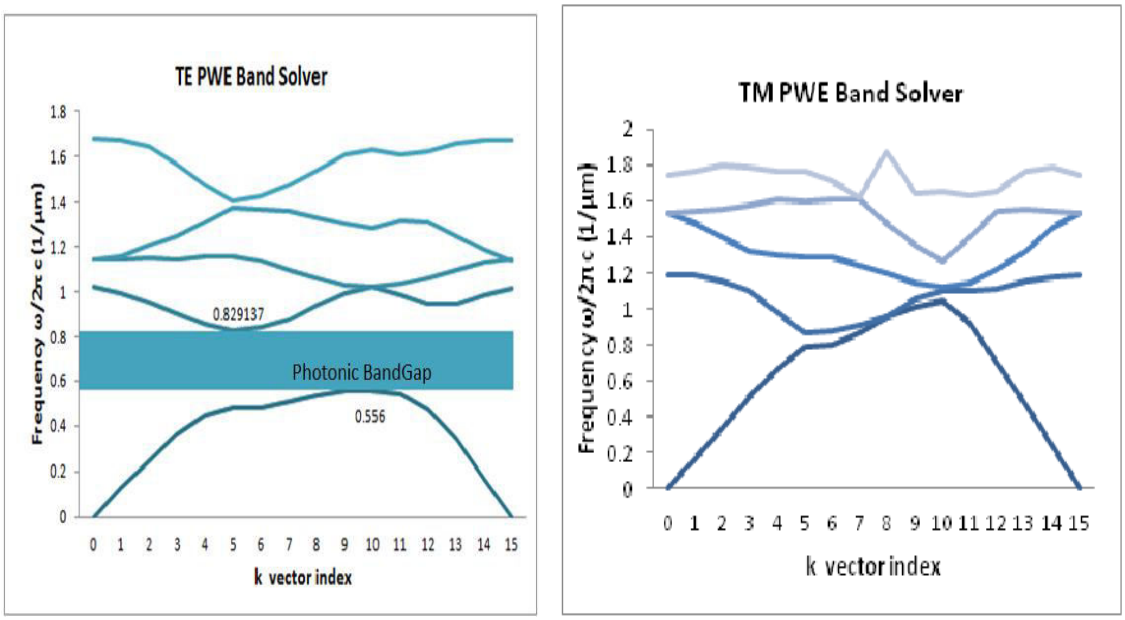

(a) (b)

Figure 3.2(a) TE Bandgap for defect-free crystal using PWE Band Solver. Shaded area is the bandgap. **(b)**TM Band Solver for defect-free crystal, showing no bandgap in TM modes.

The introduction of the defects in the photonic crystal introduces the guided modes within the photonic bandgap, thus allowing the propagation of light signal along the waveguides. These guided modes are categorized into even-like and odd-like supermodes as shown in fig. 3.3(a) and fig. 3.3(b) for the DC structures given in fig. 3.1(b) and fig. 3.1(c) respectively.

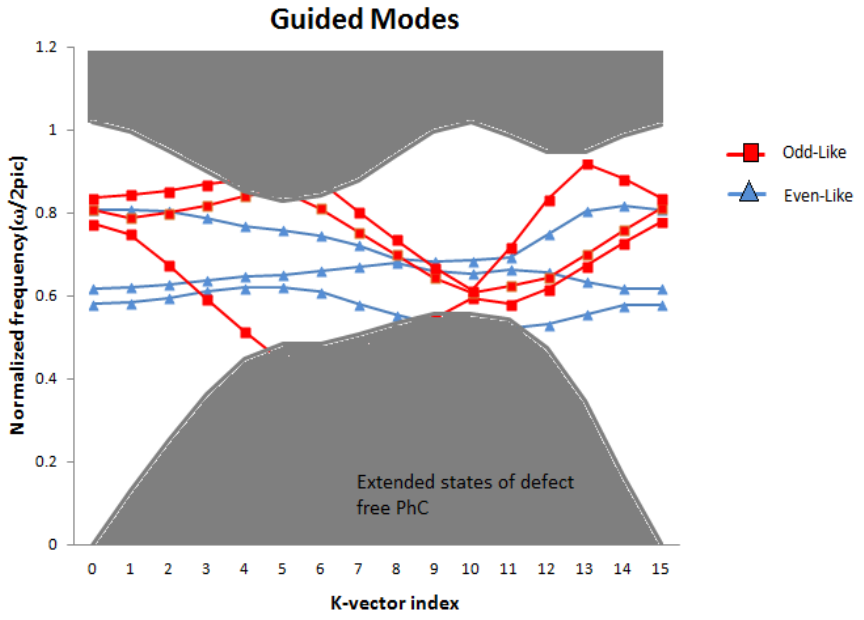

(a)

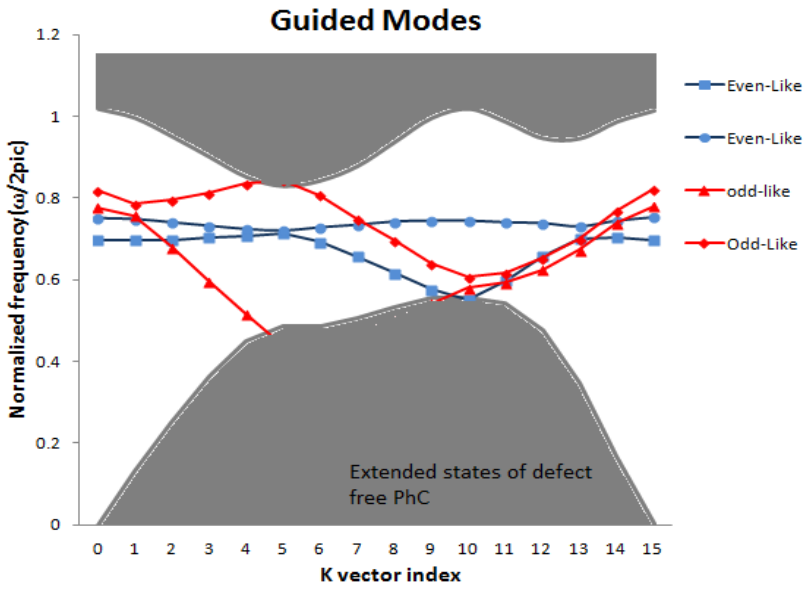

(b)

Figure 3.3(a) Guided modes for square lattice DC structure with a ring cavity defect at the bend. **(b)** Guided modes for square lattice DC structure with a semicircular defective bend.

The dispersive nature of perturbation due to supermodes is studied and analyzed with the help of group velocity curves of both even-like and odd-like modes for configuration given in fig. 3.1(c). The purpose of the graph in fig. 3.4 is to visualize the deviation between the group velocities of two modes separated from a single guided mode travelling inside the waveguide and the non-uniformity arising due to presence of these supermodes. As the slope of group velocity curve increases with the increase in frequency, more distortion can be observed. The perturbations in the coupler can be explained with the help of coupled mode theory [53], which explains the coupling and exchange of power among the guided modes. Coupled mode theory treats both the waveguides, i.e. waveguide A and waveguide B as an individual component waveguides affected by the presence of each other.

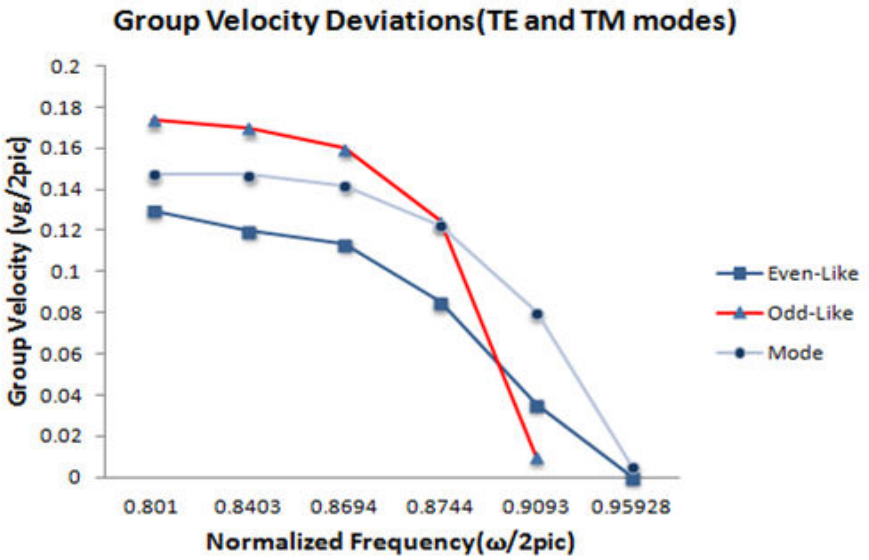

Figure 3.4 Group velocity deviation of even-like (marked by squares) and odd like (marked by triangles) supermodes from the original guided mode (marked by circles).

Coupling coefficient is calculated from the k-vector of guided even-like and odd-like modes as shown in fig. 3.5. The k-vector scale is indexed from 0 to 15 in the region [0-2π/a] (where 'a' is the lattice constant) in the band diagrams, where all k-vectors are unique, i.e. this is a set of non-equivalent wave vectors closest to the k vector = 0 (origin), a region called the first Brillouin zone [1]. Coupling coefficient calculated, indicates the absolute difference between the k-vectors of even like and odd like modes.

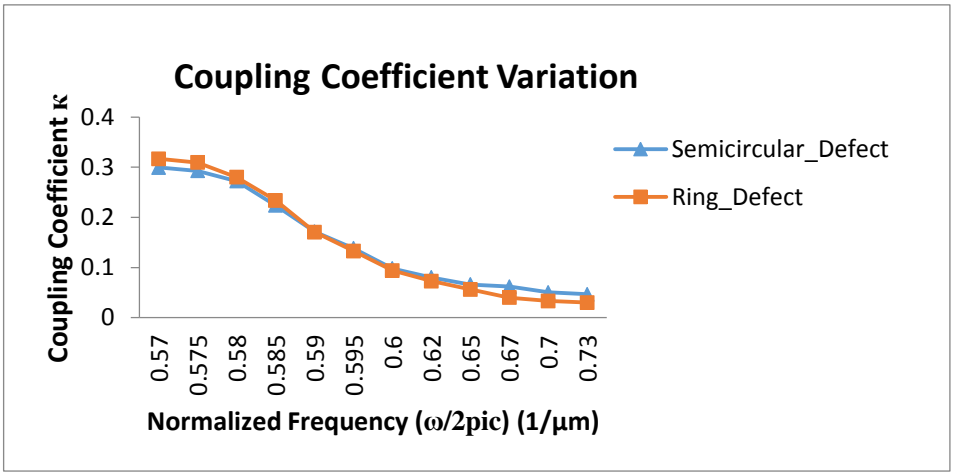

Figure 3.5 Coupling coefficient variation with respect to the frequencies for the ring defective bend and the semicircular defective bend directional couplers.

The graph in the fig. 3.5 shows the comparison of the coupling coefficients with respect to the normalized frequencies for the given DC structures in fig. 3.1(b) with ring defective bend and fig.3.1(c) with semicircular defective bend. More the coupling coefficient,

higher is the coupling. At the operating wavelength of 1467.1 nm, (i.e. at 1/λ= 0.681), the coupling coefficient for the configuration in fig. 3.1(c) equals to 0.057 and for configuration in fig. 3.1(b) equals to 0.037 in the units of propagation constant. Therefore, the former configuration with semicircular defective bend is better coupler with higher coupling coefficient.

Fig. 3.6 shows the comparison of coupling lengths of the DC structures in fig. 3.1(b) and fig. 3.1(c) with respect to the normalized frequencies. Coupling length is the inverse of coupling coefficient, converting the units from k-vector to the length units. The Plane Wave Expansion (PWE) method compares the band frequencies with respect to the k-vector index. We however calculate the coupling length by converting the x-axis scale of k-vector index (0 to 15) to the scale of the original k-vectors (in the range of 0-2π/a; the first Brillouin zone) where 'a' is the lattice constant. At operating wavelength 1467.1 nm, with 1/λ equals to 0.681, we have coupling length for configuration in fig. 3.1(c) equals to 109 µm, shorter than the configuration in fig. 3.1(b) with coupling length equals to 167 µm. It shows that configuration having larger coupling coefficient, needs shorter coupling length as it is a better coupler.

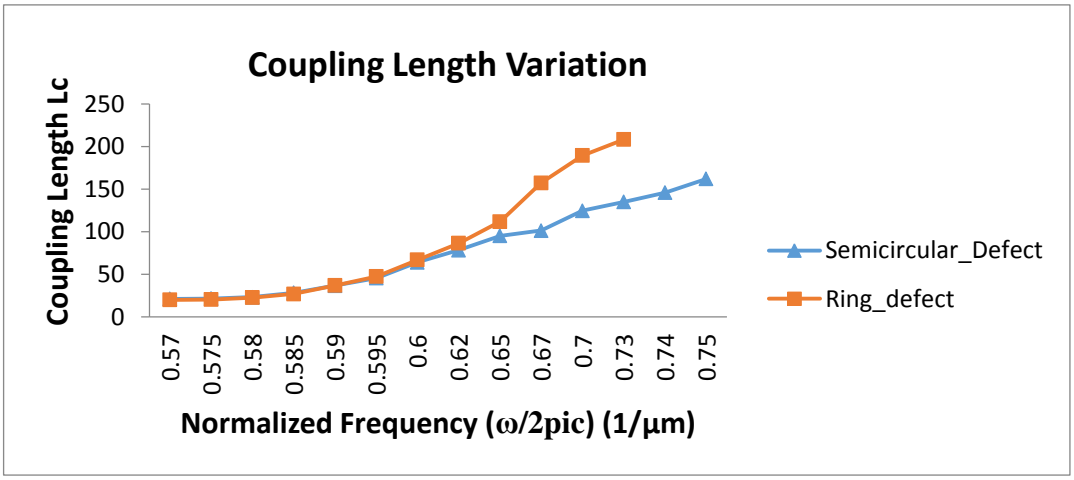

Figure 3.6 Coupling Length variation with respect to the frequencies for both ring defect and semi-ring defective structures.

Table 3.1 summarizes the differences between results of two DC configurations as given below.

Table 3.1 Comparison of coupling parameters for the two DCs.

	Coupling Coefficient(in the units of k)	Coupling Length (in µm)
Directional Coupler (ring defect)	0.037	167
Directional Coupler (quasi-ring defect)	0.057	109

Transmittance curves for configuration in fig.3.1(c) are analyzed using FDTD method [54] as shown in fig.3.7. The graph shows the normalized power distribution among the throughput port, coupling port and the power reflected back through waveguide B. This configuration with semicircular cavity defect at the bend performs the best as a 3-dB coupler, dividing the input power into throughput and coupled port equally (~50% of the total output power) with reflection losses less than 6% of the total input power. With ring cavity as shown in fig. 3.1(b), reflected power losses are more than 12.5% of input power. The operational bandwidth calculated for this 3-dB directional coupler is calculated as 37.5 nm (1.448µm – 1.4855 µm) and the quality factor is 39.1. Higher the quality factor, lesser is the rate of energy losses.

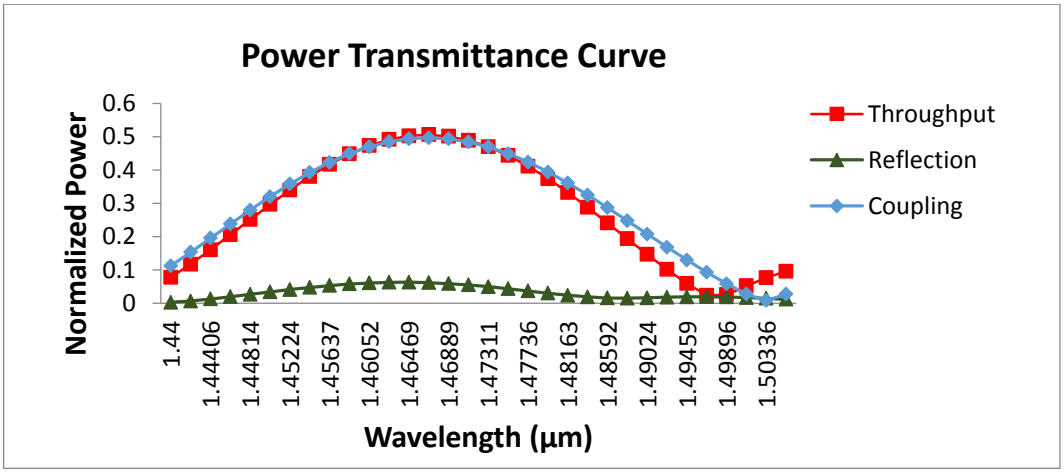

Figure 3.7 Power transmittance curve for the semicircular defective bend DC configuration.

Fig.3.8 shows the electric field (E_y) propagation of the light signal in the 2D DC crystal layout with semicircular defective bends in X-Z plane. In this figure, it can be seen that the reflector rod added in the waveguide A directs the signal power towards the coupled waveguide, thereby equalizing the distribution in both the waveguides. Also, at the bends, efficient power transmittance can be observed.

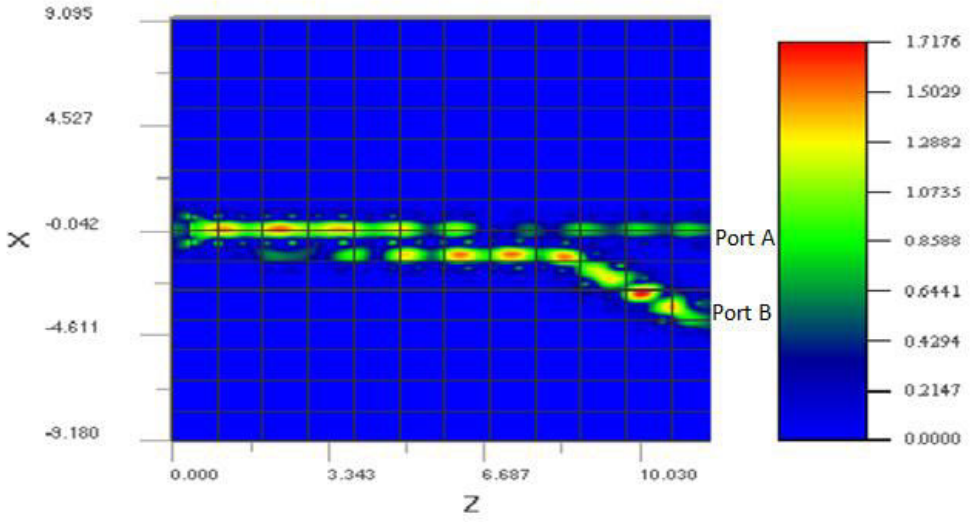

Figure 3.8 Electric Field Propagation profile of the semicircular defective bend DC configuration in a crystal layout.

The power distribution of the directional coupler among the two ports discussed can be varied in percentage (other than the 50% distribution in 3-dB coupler) by changing the number of reflector rods in waveguide A or by varying the position of silicon rod raised towards the bend below waveguide A along the arc of the bend shown with an arrow in fig. 3.1(a). However, the radii of the rods in the centre of semicircle cavity or in the bends do not have much role in the variation of power distributions.

3.5 CONCLUSION

Directional coupler on a 2D square photonic crystal lattice is designed and simulated as a 3-dB coupler. Two configurations with different defect cavities are compared on the basis of parameters measuring their coupling strength. The directional coupler structure designed in fig. 3.1(c) has a better coupling strength with the coupling coefficient equal to 0.057 than the coupler in fig. 3.1(b) with the coupling coefficient of 0.037 (in the terms of absolute difference in the k-vector or the propagation constants) at the operating wavelength. The coupling length of the former, calculated to be 109 µm is lesser than the DC in fig. 3.1(b), which is equal to 167 µm. Shorter the coupling length, higher is the coupling coefficient i.e. better the coupling and lower losses. Power transmittance curve is studied for the better configuration (fig. 3.1c) showing throughput and coupling power outputs equally distributed (≈50% of the total output power) and the maximum reflection losses less than 6% of the total input power. Also, the bandwidth calculated in the S-Band window is 37.5 nm.

CHAPTER 4
DESIGN OF PHOTONIC CRYSTAL ADD-DROP FILTERS BASED ON QUASI-RING CAVITIES

The design of add drop filters on two dimensional square photonic crystal lattice is investigated in this chapter. The filters are based upon multiple quasi-ring cavities inside the square cavity. The theoretical power transmittance spectra are analyzed using Finite-Difference Time-Domain (FDTD) approach for two alternative add-drop filter (ADF) layouts. The drop efficiency of 95% is achieved with one of the filters having perfect backward drop at the wavelength of 1.48 μm. The minimum spectral width attained is 68 nm. The size of this device is 12.4 μm × 12.4 μm. Thus these filters can find their application in ultra compact photonic circuits and bio-sensing circuits as multiple cavities can easily trap the bio-molecules within them.

4.1 INTRODUCTION

Since the photonic crystal devices have made a significant contribution in the areas of compactness, miniature sizes and fast switching etc., many add drop filters (ADFs) are also designed using photonic crystals. The ADFs are an essential component of various optical circuits such as multiplexers/de-multiplexers, modulators, switches etc. They consist of two straight waveguides i.e. bus waveguide and drop waveguide, having resonating cavities sandwiched between them.

The ADFs are coupling devices, in which light launched into bus waveguide tunnels through the resonating cavities to drop waveguide and exits through one of its ports. If the light output exits in the direction parallel to the input light, it is known as forward dropping. Whereas if the light exits anti-parallel to that of input light; it is backward dropping. The filters based on resonating cavities are suitable candidates for wavelength division multiplexing (WDM) communications as they provide better drop efficiency for a given size of a structure [23]. The coupled resonators in cascade help in further improving the individual resonator characteristics [55].

Ahmed Taalbi et al. [19] demonstrated the filter characteristics for single-ring and dual-ring configurations based on 2D triangular lattice photonic crystal (PC) silicon rods. P. Andalib et al. [20] designed the new ultra compact ADF based on the 2D triangular

lattice. The resonator is formed by two coupled curved Fabry-Perot cavities in the glass background. M. Djavid et al. [24] investigated the multi-channel drop filters based on the square lattice. The drop efficiency of this three drop ports filter at resonant wavelength is 81%.

In the above literature, various add/drop filters based on both triangular and square lattices are discussed. The ADF having dual curved resonator based on triangular lattice [19] shows a trade-off between drop efficiency and size of the structure. In this dual structure, two ring resonators are cascaded vertically to obtain the complete transfer of light towards the drop waveguide. Although, the cascaded device has higher drop efficiency than a single resonator, it increases the size of structure. The Fabry-Perot cavity resonator discussed [20] has drop efficiency of 68% only. However this hexagonal lattice structure has an advantage of larger overlap between the cavities and the other defects due to curved formation of cavities.

The curved resonator trend of Fabry-Perot cavities [20] can be applied to the square photonic crystal lattice also as more subtle defects can be introduced in the orientation angle between two square lattice vectors as compared to the hexagonal lattice. In this chapter, we discuss two new ADF configurations based on square photonic crystal lattice. This device is formed by curved quasi-ring cavities inside a square cavity, placed in between the bus waveguide and drop waveguide. Various defects are introduced at corners of the cavity to reduce the reflection losses. The transmittance spectrum is analyzed and compared for both the configurations. The curved resonating cavities have an advantage of miniature sizes than multi-ring resonating structures as the curved cavities do not require two separate resonators for better coupling efficiency.

4.2 SIMULATION SET UP

The add drop filters (ADF) are designed on a 2D square lattice in X-Z plane. The silicon rods of refractive index 3.47 are placed in air wafer. Lattice constant for ADF is taken in the range of 5.378 μm to 5.382 μm and radius of rod is 0.172 times the lattice constant. Two straight waveguides are formed with the introduction of line defects by removing a series of rods. The input waveguide is the bus waveguide and the coupled waveguide is the drop waveguide which outputs the light of a specific wavelength to one of its ports. We have designed square resonating cavities consisting of two semi curved reflectors as shown in fig. 4.1(a) and fig. 4.1(b). The input wave is the Gaussian modulated wave.

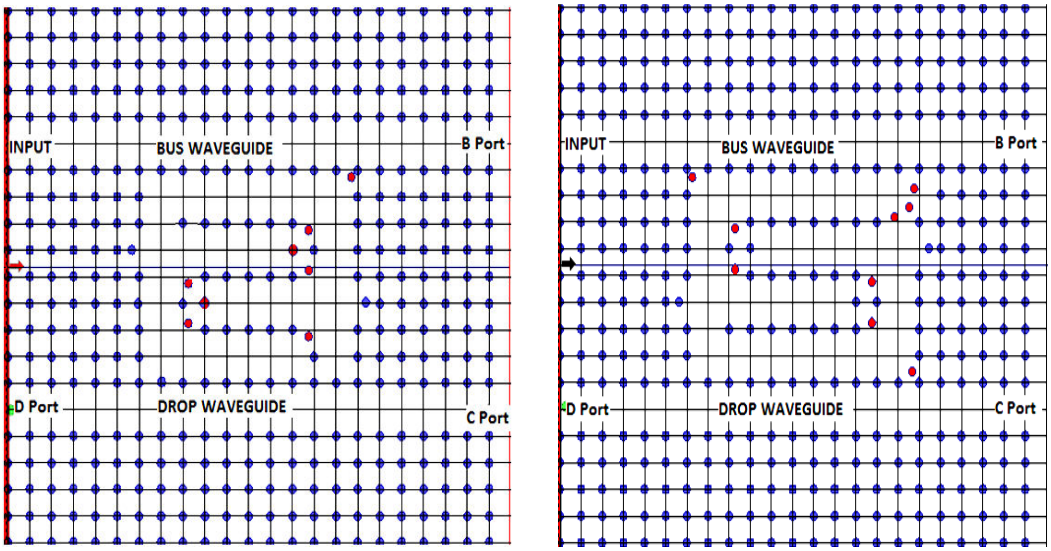

(a) (b)

Figure 4.1(a). Add drop filter configuration (A). **(b)** Add drop filter configuration (B).

All the rods marked red in fig. 4.1 are defected rods and are displaced from their original positions to form the cavities. Scatterer rods are added to the selective corners to reduce the reflection losses. The corners facing open ends of the cavities have no scatterer rods. The Gaussian input is launched into bus waveguide through the vertical arrowed input plane at left end of the layout marked with red color. The ports labeled as B, C and D are the output ports.

The square resonating cavity between the waveguides has multiple quasi rings curved inside it as shown in fig. 4.1(a) and 4.1(b). The two configurations however differ in the direction of curves formed by the resonating cavities. The cavities in both configurations are facing opposite to each other. These ADFs are designed for backward dropping of the particular wavelength i.e. the light of that wavelength is completely guided towards the D-port of drop waveguide with negligible transmission through B and C port. ADF (A) has lower end terminated to the drop waveguide to enhance backward coupling at the resonant wavelength. Similarly ADF (B) has upper end terminated to the bus waveguide to improve the coupling efficiency, as the coupled light that travels through this passage otherwise suffers high reflection losses at the ends without its termination. This termination leads to the smooth transition of light through the bends and turns, thus lowering the losses.

4.3 RESULTS AND DISCUSSIONS

The Photonic Band gap (PBG) for designed ADF devices is calculated using PWE method [52]. The TE modes band gap for the defect-free ADF configurations lies between the range 1/λ (1/µm) equals to 0.5693 - 0.8378, which represents the range of wavelengths from 1.193 to 1.756 µm. However, no band gaps are found in TM modes.

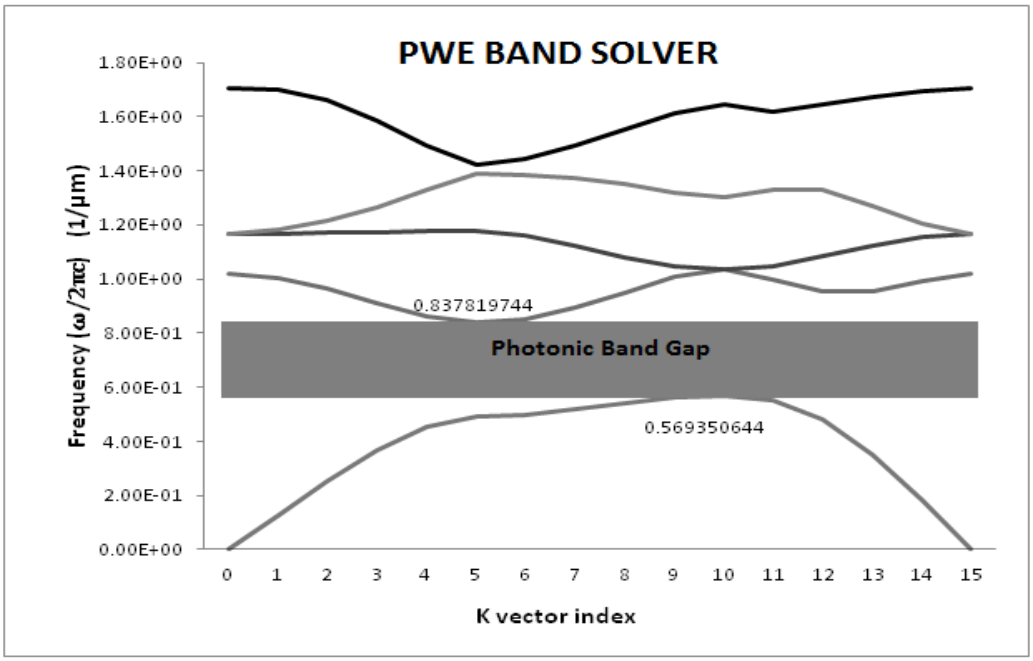

(a)

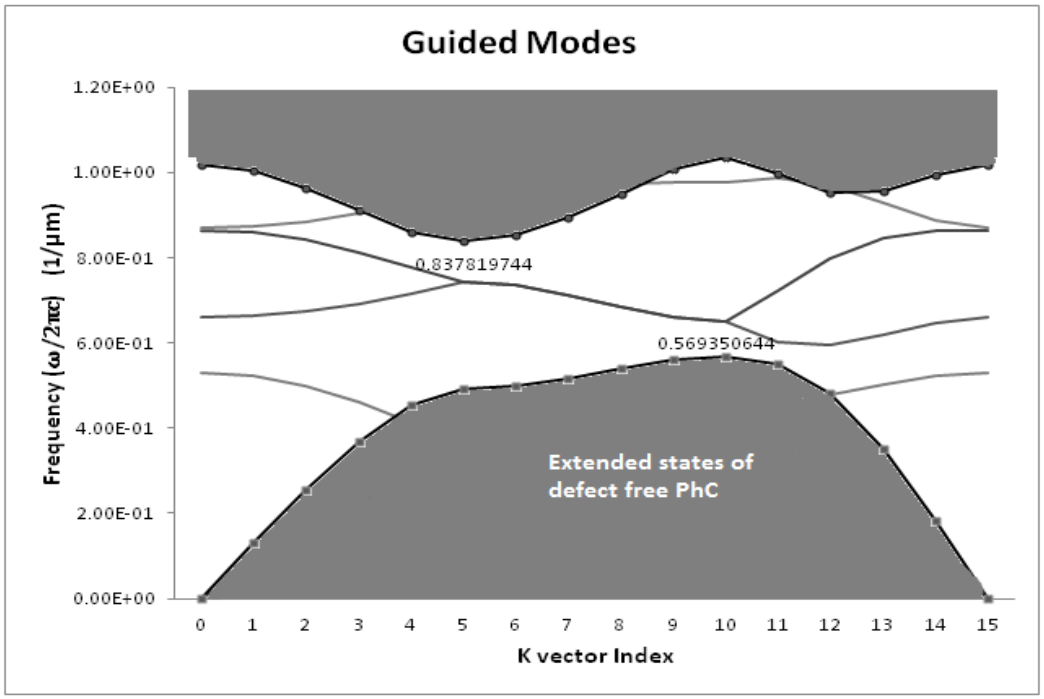

(b)

Figure 4.2 (a) TE modes Photonic Band gap for defect-free photonic crystal. **(b)** Guided TE modes of the photonic crystal with line-defects (i.e. the waveguides in the ADF circuits).

The introduction of line defects in the photonic crystal introduces guided modes within the photonic band gap as shown in fig. 4.2(b), thus allowing the propagation of light signal along the waveguides in the ADFs given in fig. 4.1. Thus, these ADF structures are simulated by launching the input Gaussian wave of 1.5 µm through the vertical input plane as this wavelength of 1.5 µm lies in the band gap and therefore it is guided efficiently through the waveguides in ADFs.

The transmission spectrum of the two ADFs are simulated using the FDTD method [54] for the calculation of light transmittance through various output ports at the wavelength of 1.5 µm. Light dropping efficiencies are analyzed by visualizing the transmittance spectra as given below in the fig. 4.3 and fig. 4.4. In fig. 4.3, it shows the electric field distribution (Ey) image maps of the ADF layouts placed in the X-Z plane and fig. 4.4 calculates the transmittance spectra curves showing the power distribution for both the layouts.

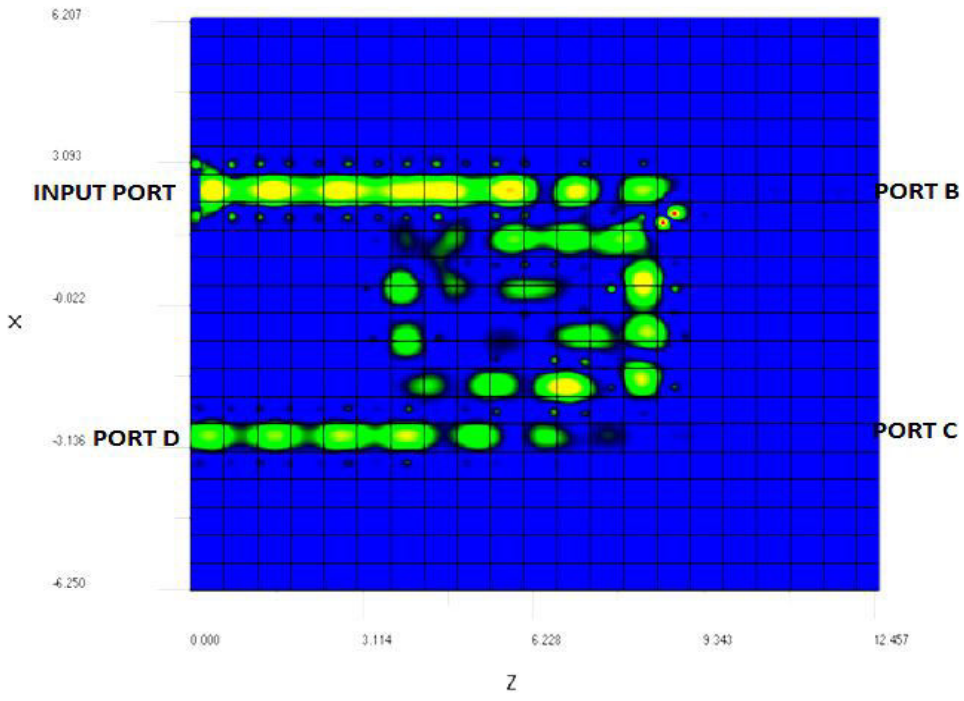

(a)

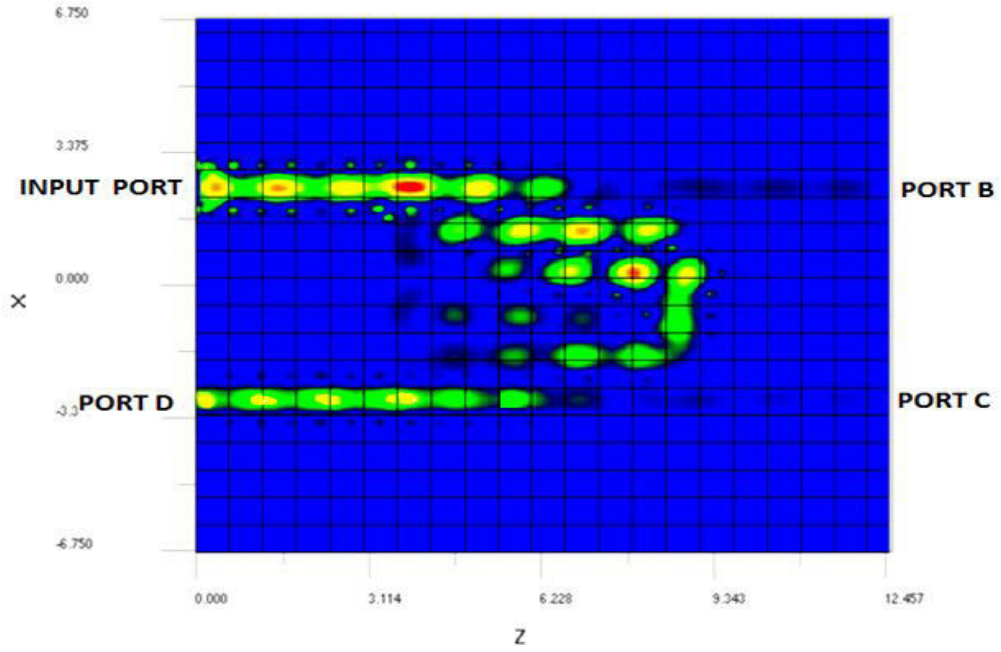

(b)

Figure 4.3(a) Electric field distribution Image Map for ADF (A). **(b)** Electric field distribution Image Map for ADF (B).

Image maps show significant variation in the field distribution as backward dropping of the input light at the operating wavelength of 1.5 µm is shown. The difference in behaviour of both the ADFs can be analyzed further with the help of transmittance curves as shown below in fig. 4.4.

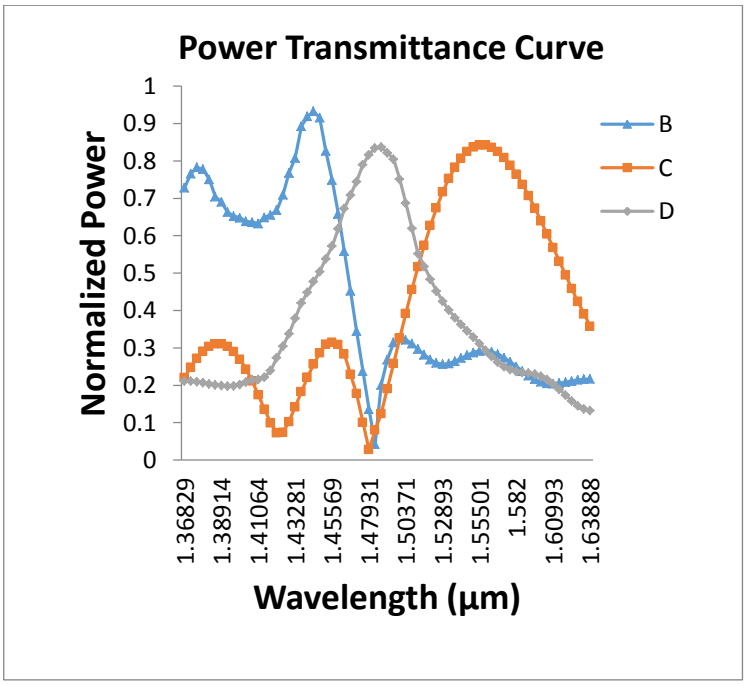

(a)

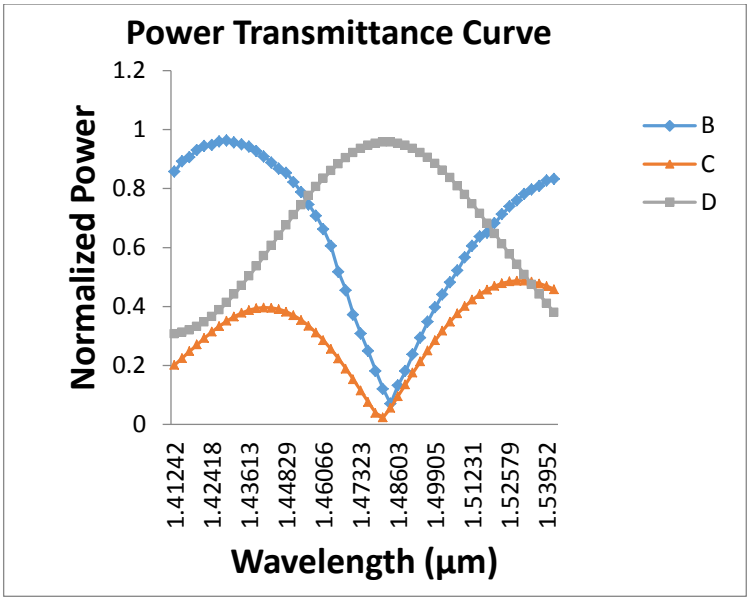

(b)

Figure 4.4 (a) Power transmittance spectra for ADF (A). **(b)** Power transmittance spectra for ADF (B).

From the fig. 4.4, it is observed that ADF (B) has better dropping efficiency than ADF (A). Maximum normalized power at the backward dropping wavelength for ADF configuration B is 95 %, whereas it is 83% for configuration A. However, the perfect power transfer takes place in both cases, i.e. at the wavelength (λ) equals to 1.483 µm, the output is obtained at port D with negligible transfer of light to the other ports. ADF (A) has spectral width of 68 nm for backward dropping whereas ADF (B) has 95 nm. Selectivity of ADF (A) is better than ADF (B) by 28%. ADF (A) has negligible transmission through port B after the wavelength is increased beyond 1.4478 µm. The light backward drops through the port D in the range 1.447 µm – 1.516 µm, and beyond it, light is completely transferred to the port C.

4.4 CONCLUSION

The two ADF configurations designed in this chapter are simulated and analyzed using FDTD approach. The square cavity with multiple curved cavities inside is introduced in this design. The configuration ADF (A) has an output efficiency of 83% at the port D whereas spectral width of this configuration is 68nm. And ADF (B) has an output efficiency of 95% at the port D but the spectral width of this configuration is 95 nm. Therefore, if coupling is improved to enhance the drop efficiency, the spectral width also increases, thereby reducing the quality factor. However, perfect drop is observed in both cases. The size of the design is 12.4 µm × 12.4 µm which is very suitable for integration in the miniature sized devices.

CHAPTER 5
DESIGN AND ANALYSIS OF 2D PHOTONIC CRYSTAL WAVELENGTH ROUTERS USING MICRO-RIDGE AND ARC WAVEGUIDES

In this chapter, (1x2) T-shaped wavelength router is devised on two dimensional square photonic crystals lattice. The conventional tapered ridge waveguides and arc waveguide of comparatively low dielectric constant are introduced in the crystal structure. These waveguides facilitate the light transmission from the input port to output ports. The transmission spectrum for this structure is analysed using Finite-Difference Time-Domain (FDTD) approach. The simulation results indicate that the designed router can separate the wavelengths of 1.52 µm and 1.6 µm with the power efficiency as high as 99.9%. The minimum crosstalk obtained for the router is -29.48 dB. This device is highly suitable for integrated circuits owing to its simple structure.

5.1 INTRODUCTION

As we know, the photonic crystal devices have made a significant contribution in the areas of compactness, miniature sizes and fast switching etc., many wavelength routers are also designed using photonic crystals [37], [33]. Wavelength routers are one of the building blocks of optical switch circuits. The routers route the signal launched at the input port to different output ports based on the wavelengths constituting the signal. This routing mechanism is obliged by the resonant wavelengths of various routing elements present along the transmission path of the signal. Therefore, the input signal is de-multiplexed into different resonant wavelengths and these wavelengths are optically switched to their respective output ports.

Photonic crystal routers consist of straight waveguides, formed by removing a series of crystal rods. The resonating cavities are also introduced in the routers to improve their selectivity [37]. Crosstalk is an important parameter for the analysis of performance of routers as it is the degree of interference of two signals. The crosstalk between two ports can be calculated as the difference in the transmittances in decibels, i.e. $CT_{i,j} = T_j - T_i$, where CT_{ij} is the crosstalk between port ‘i’ and port ‘j’ and T_i, T_j are the transmittances of ports ‘i’ and ‘j’ respectively [29].

Giovanna Calo et al. [29] devised the (1x2) basic cross wavelength routers based on photonic crystal ring resonators. A number of such routers are assembled into a single structure to form higher order router matrices. Authors have designed the resonant ring structures, which can be tuned by varying the radius of central rods of ring to optimize the performance of routers. Wei Yu Chiu et al. [33] demonstrated the silicon on insulator 2D ring resonators based on hexagonal photonic crystal lattice. These ring resonators act as routers, routing the two wavelengths of 1.31μm and 1.55 μm to their respective output ports. The nano structures of this device are fabricated using E-beam lithography technique. Authors have optimized the radius of nano-rods to reduce optical loss and crosstalk problem.T. N. Bakhvalova et al. [56] proposed and investigated the 2D photonic de-multiplexer which outputs different wavelengths used in telecommunication. Authors have introduced various nano filters such as defective rods, tapered waveguides etc. within the photonic crystal T-junction waveguide to have selective radiation of light. These nano-devices modify the behaviour of a structure to a large extent.

In the above literature, various routers are analysed for their performance as a switching device. The (1x2) broadband router discussed [29] is scalable and is also used in (4x4) configuration using eight such routers. The minimum crosstalk obtained for this router is approximately -16dB within the range of 1.48 μm -1.55 μm. The ring resonator device illustrated in [33] has conventional silicon ridge waveguides at the input and output ports for ensuring the lossless transition of light into and from the photonic crystal waveguide. The advantage of the de-multiplexer demonstrated in [56] is its miniature size. However this device has low drop efficiency and low insulation.

In this chapter, we have designed the wavelength router based on 2D square photonic crystal lattice having Si rods embedded in air wafer. The conventional photonic waveguides of relatively lower refractive index ($Si0_2$) are introduced at various points in the photonic crystal waveguides (air). These waveguides break the periodicity of photonic crystal and direct the input signal towards the output ports with extremely low losses. It is due to the total internal reflection phenomenon suffered by light rays in these guides. The transmission spectrum of router is analyzed using FDTD approach. The crosstalk between two outputs is also calculated as it indicates the degree of interference between different signals.

5.2 SIMULATION SET UP

The wavelength router is designed on the square photonic crystal lattice (in X-Z plane) having Si rods of refractive index 3.47 placed in an air wafer. The substrate is made up of quartz (Silica) having refractive index of 1.45. A T-shaped wavelength router is formed by removing the silicon rods from the crystal in a straight line, thus introducing the line defects. One complete horizontal straight waveguide and the other quasi vertical waveguide intersect to form the T-shape as shown in fig. 5.1(a). Also, the conventional photonic waveguides of refractive index same as substrate (quartz) are introduced in the router, i.e. two tapered ridge waveguides are placed towards the output ports and an arc shaped waveguide is placed exactly at the middle of the T-junction. Both of these waveguides have height of only 1µm in the vertical Y-direction. The radius of silicon rods in the crystal is 0.32 times the lattice constant 'a', where the lattice constant for this router is 0.682 µm.

Above the tapered ridge waveguides, are placed the defective silicon rods marked in red color in fig. 5.1(a), having half the radius of the crystal rods. The ports marked as 'right' and 'bottom' are the output ports and input signal is launched through the port marked as 'input'. To the extreme left of the structure in fig. 5.1(a) is the red colored vertical input plane. The input signal is launched in the +z direction through this plane. In the fig. 5.1(b) and 1(c), the top and side view of designed router is shown, in terms of the variation of refractive index in the vertical Y-direction. Silicon rods of higher refractive index are appearing in the red color at the top, whereas the substrate and the conventional waveguides are in the blue color, which are of lower refractive indices of 1.45.

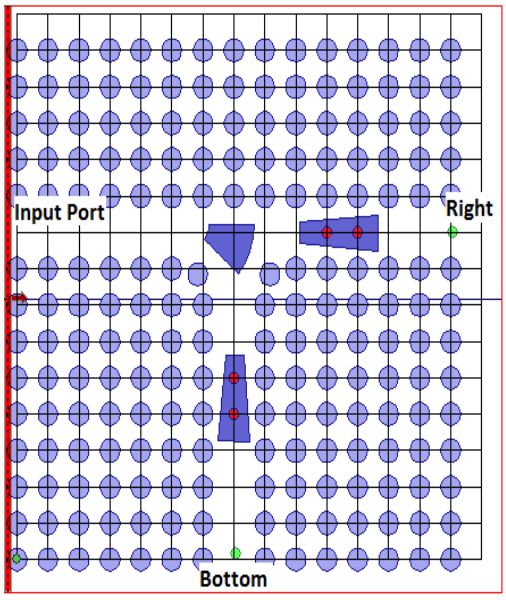

(a)

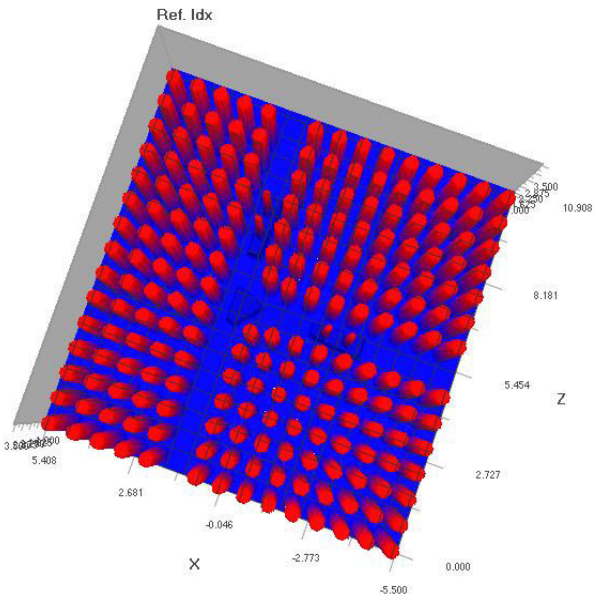

(b)

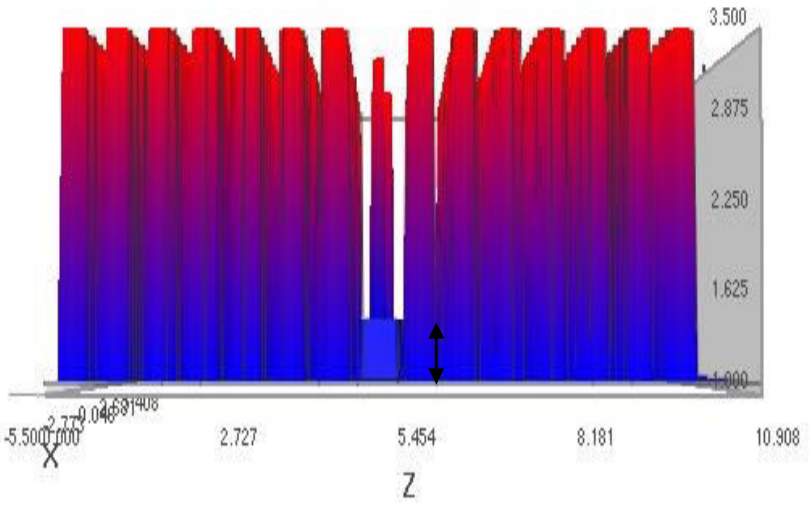

(c)

Figure 5.1 (a) Simulation setup of the wavelength router. **(b)** 3D Top view of the router structure. **(c)** 3D side view of the router (ridge waveguide of 1µm is marked with a black arrow having silicon rods above it).

The significance of conventional waveguides in this structure is their ability to guide light through the mechanism of total internal reflection. Where photonic crystals provide efficient confinement for the light signal owing to their band-gap, the conventional waveguides are placed in the air as light easily scatters in the low index material. Thus the quartz base below the defective rods inside the photonic waveguides not only provides the vertical confinement but also reduces the scattering losses. The tapering of ridge waveguides is done towards the intersection. The defective silicon rods above the ridges are responsible for good selectivity of the router. The arc waveguide at the intersection is mainly for smooth transition of input signal towards the output ports. The variation of output signal with change in arc radius is also studied in this work.

5.3 RESULTS AND DISCUSSIONS

Photonic band-gap for the designed wavelength router is calculated using Plane-Wave Expansion method (PWE) [52].The TE modes band gaps for the defect-free router configuration lie between the ranges 1/λ (1/µm) equals to 0.57438 - 0.712168 and 0.3299-0.413818. We consider the first band gap having higher frequencies i.e. 0.57438 - 0.712168 (1/µm) which represents the range of wavelengths of our interest i.e.1.404 to 1.741 µm. However, no band gaps are found in TM modes.

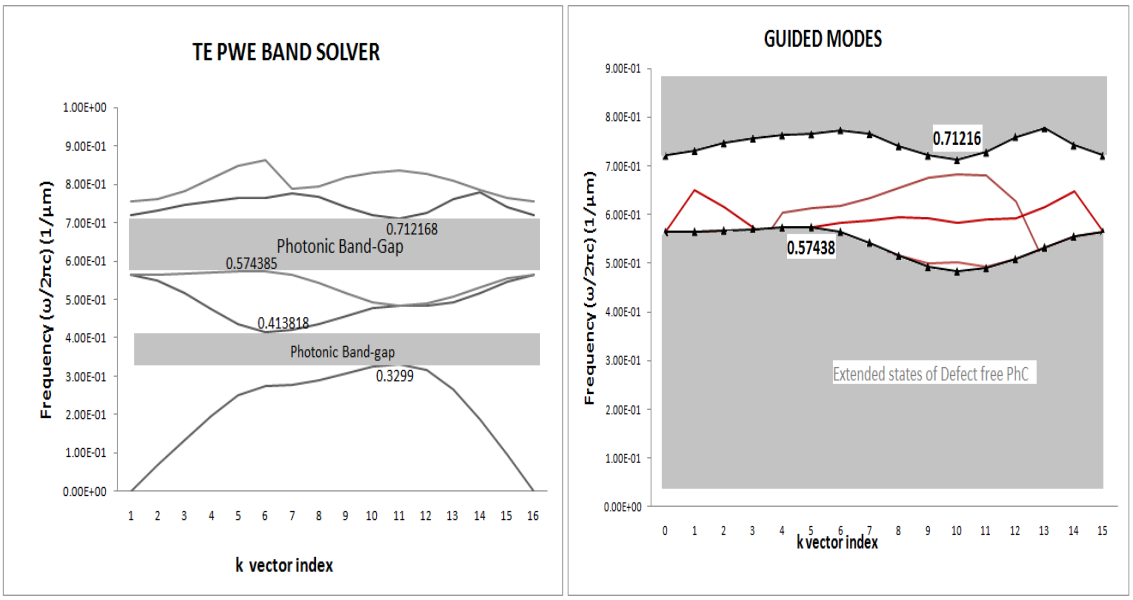

(a) (b)

Figure 5.2 (a) TE Photonic band gap of defect free photonic crystal router. **(b)** Guided TE modes of wavelength router with defects (shown as red lines) within the first band gap.

With the introduction of line defects in the photonic crystal to carve a T-shaped junction router, the photonic band gap disappears with the inception of guided modes inside it. The propagation of these light modes is possible within the waveguides formed by defects. In fig. 5.2(b), guided transverse electric modes are shown in red color. The grey shaded region is representing the extended states of defect free crystal, i.e. this region has no change in the band structure even after defects are formed, except the band gaps no longer exist.

The power transmission curves are calculated using Finite-Difference Time-Domain approach [54]. The efficiency of designed wavelength router is optimized by changing the radius of an arc in the middle of T-junction. The variation of maximum power output efficiency for both the output ports with an arc radius is studied as shown in fig. 5.3. The results show that maximum power efficiency is attained for the radius of 0.892 μm, where right port has 99.9 % and bottom output port has 99.5% output efficiency. Therefore, the complete transmission spectrum for the router is analyzed at the radius of 0.892 μm as discussed below.

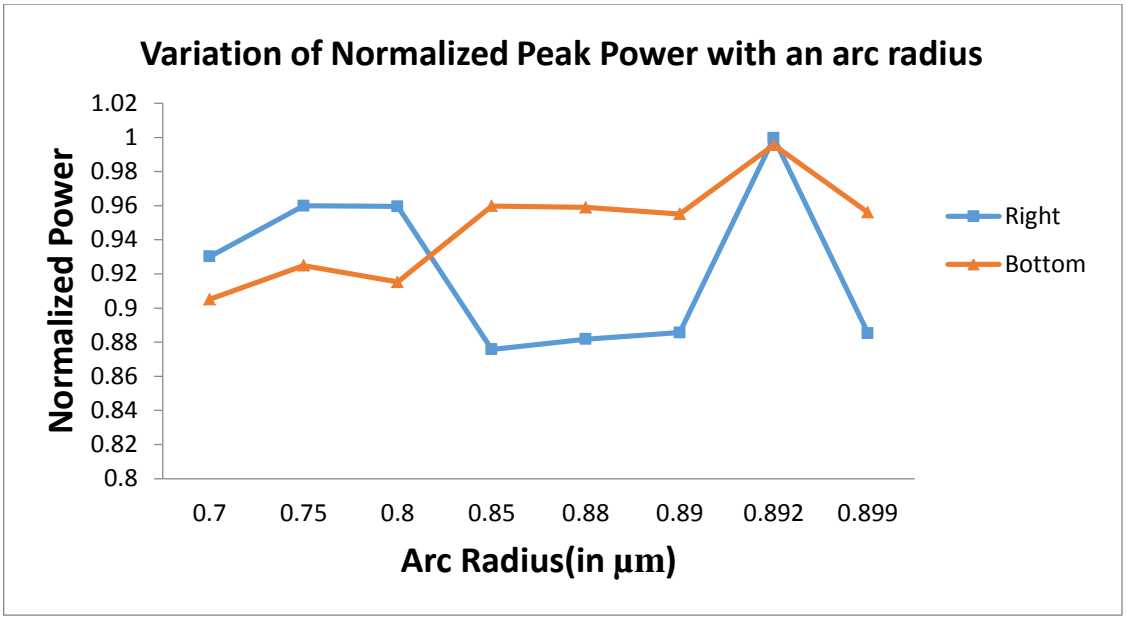

Figure 5.3 Variation of peak normalized power with change in an arc radius.

The transmission spectrum of wavelength router is shown in fig. 5.4. In fig. 5.4(a), the power spectrum is plotted, which is normalized with respect to the input plane. The results show the maximum throughputs of 0.999 and 0.995 are attained at the wavelengths 1.52 µm and 1.6 µm for right and bottom port respectively. The value of crosstalk is also calculated between the output ports at these two operating wavelengths of the router from the fig. 5.4(b).

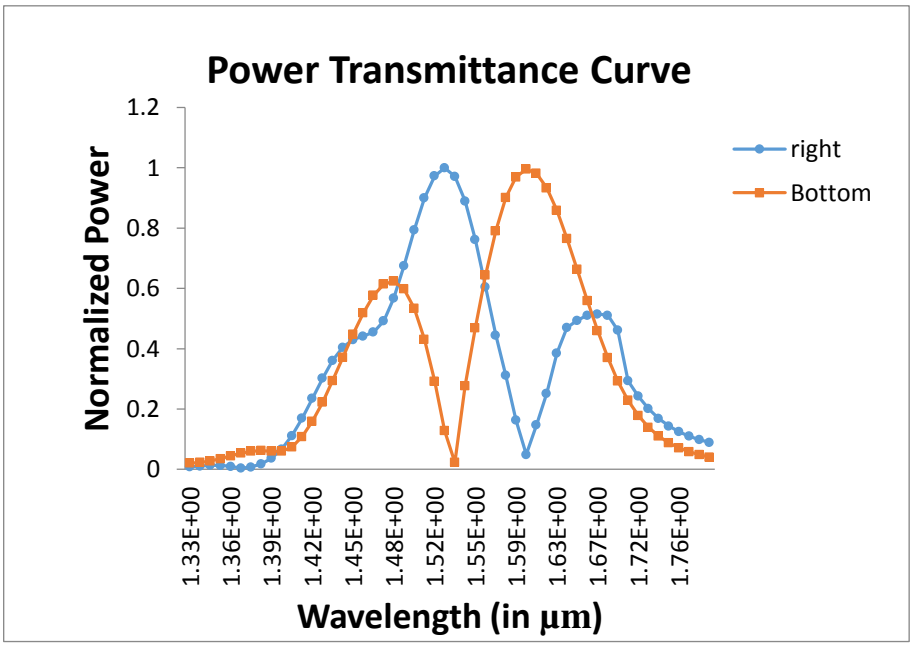

(a)

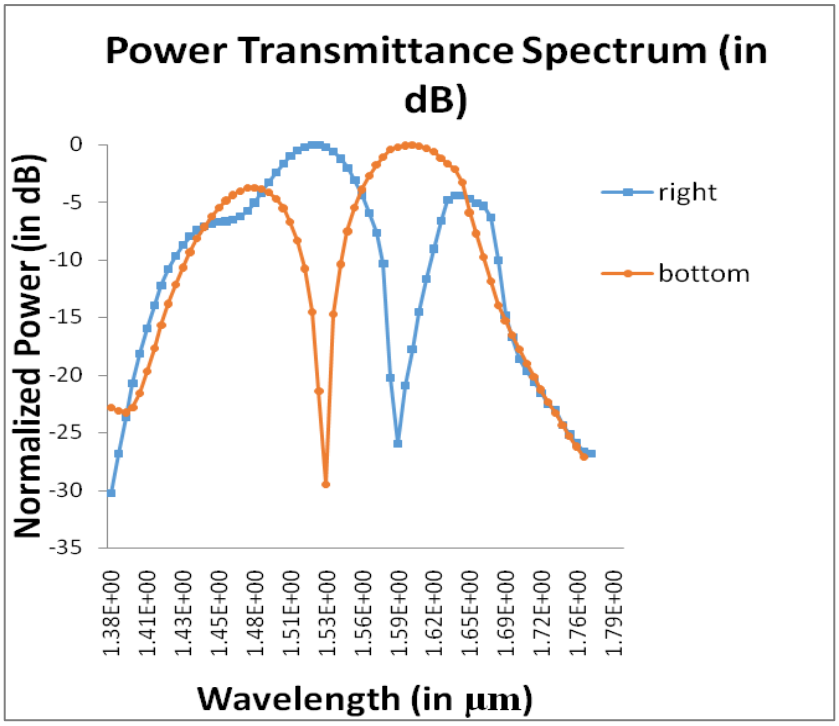

(b)

Figure 5.4 (a) Normalized power transmittance curve of router with an arc radius of 0.892 µm. **(b)** Power transmittance curve of router in decibels.

From the fig. 5.4(b), to calculate crosstalk between two output ports, we have transmittances as -0.0125 dB and -29.5 dB at 1.52 µm and -0.0151 dB and -26.99 dB at 1.6 µm for the output ports present at the right and the bottom of router respectively. Crosstalk is the difference between both the outputs in decibels. For right output port at 1.52 µm, it is calculated as T_{bottom}-T_{right}, which is equal to -29.48 dB. Similarly for bottom output port, it is equal to -26.974 dB. The calculated crosstalk for both the cases is sufficiently low for an efficient performance of a router.

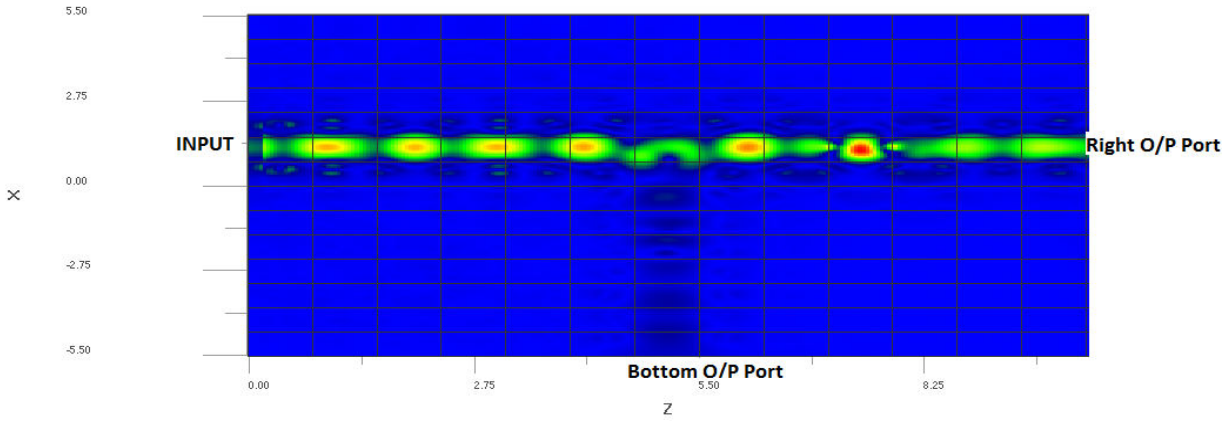

(a)

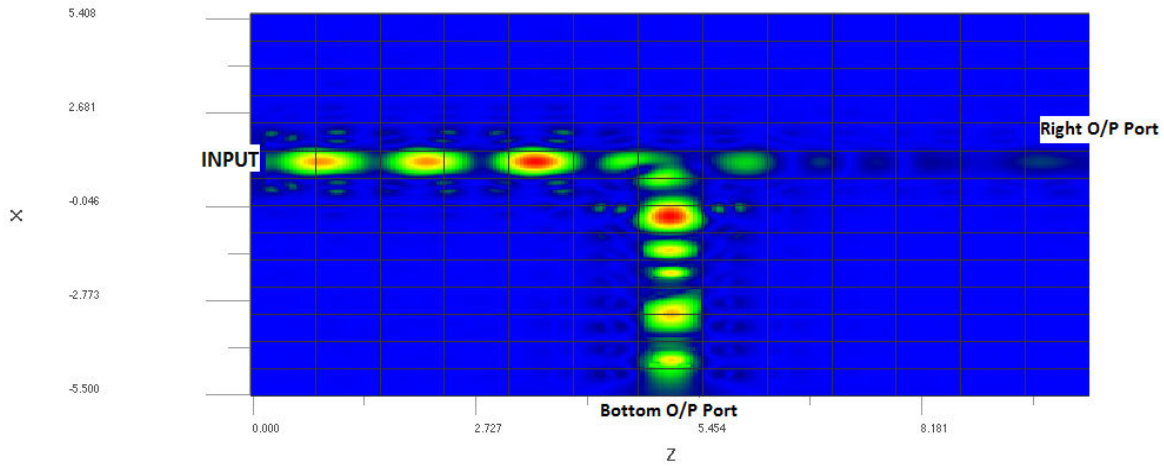

(b)

Figure 5.5 (a) Electric field distribution Image Map for wavelength router at input wavelength of 1.52 µm. **(b)** E-field Image Map at input wavelength of 1.6 µm.

The electric field image maps given in fig. 5.5 are the clear depiction of results calculated above. In fig. 5.5(a), the complete transfer of input signal power is towards the right output port of the router, simulated at the wavelength of 1.52 µm. And in fig. 5.5(b), the input power is transferred to the bottom port of the router, which is analyzed at the wavelength of 1.6 µm, showing negligible transfer to the other port.

5.4 CONCLUSION

The wavelength router configuration designed in this chapter is simulated and analyzed using FDTD approach. The conventional tapered ridge waveguides and an arc waveguide of Silica are introduced in the T-junction of photonic crystal waveguides formed. These waveguides facilitate the lossless transmission of input light towards the output ports. The designed structure splits the wavelengths of 1.52 µm and 1.6 µm to the right and bottom output ports of router respectively with output efficiency of 99% in both the cases. The minimum crosstalk calculated for this device is -29.48 dB. Therefore, this device is suitable for low loss integrated circuits with minimal interference among different outputs.

CHAPTER 6

CONCLUSION, RECOMMENDATION AND FUTURE SCOPE

6.1 CONCLUSION AND RECOMMENDATION

This chapter summarizes the results and conclusions of the defined objectives in the dissertation. The research work done is concluded as follows:

1. The first objective of designing the optimized directional coupler is achieved with the minimum coupling length of 109 µm at the wavelength of 1.48 µm. The designed directional coupler can work as a 3-dB coupler efficiently. This device finds its application in ultra-compact photonic circuits requiring high transmission efficiency as the maximum reflection losses of this device are less than 6% of the total input power.
2. We have designed two ADF configurations in the chapter 4, and one of them has drop efficiency of 95%. However, its spectral width is 95 nm. With the other ADF configuration, the spectral width is minimized to 68 nm, and drop efficiency is 83%. In both the designed configurations, perfect drop is observed at the non desirable port, where complete output is obtained at the required output port.
3. The (1x2) wavelength router discussed in chapter 5, meets our defined objective of high output efficiency as its power efficiency is 99% for both the output ports at their respective resonant wavelengths of 1.52 µm and 1.6 µm. Also, the minimum crosstalk obtained for this device is -29.48 dB for one of the output ports at 1.52 µm. Therefore, this device is the appropriate candidate for low losses integrated circuits having minimal interference among different outputs.

6.2 FUTURE SCOPE

During the course of this research, many avenues of further continuation of this work became evident. Few of them are considered worthwhile and therefore, are listed below.

1. All the photonic crystal devices in this dissertation are designed on a square crystal lattice. The performance of these structures can be analyzed on triangular or hexagonal lattice. The photonic band gaps for different lattices vary significantly. Therefore, the behaviour of a device is affected by the lattice properties to a large extent.

2. The photonic devices discussed in above chapters are all made up of silicon crystal rods in an air wafer. Whereas, many researches of various authors are based on the lattices having air holes embed into a silicon wafer. These devices can be studied for this configuration too. Silicon rods is air wafer mostly have photonic band gap in TE modes, whereas air holes in silicon wafer have band gaps in TM modes [1]. Based on this property, we can anticipate the high dissimilarity between these configurations and it can be analyzed.
3. The photonic crystal directional coupler discussed in chapter 3 and the add/drop filters in chapter 4 have wide spectral widths. Although high power efficiencies are attained, but spectral width is more. These circuits can be improved to have high selectivity.

REFERENCES

[1] J. D. Joannopoulos, R. D. Meade, J. N. Winn, *Photonic Crystals: Molding the Flow of Light*, 2nd Ed. NJ: Princeton Univ. Press, 2008.

[2] Z. Qiang, W. D. Zhou, A. Soref, "Optical add-drop filters based on photonic crystal ring resonators", *Optics Express*, *OSA* , vol. 15, no. 4, pp. 1823, 2007.

[3] V.P. Bykov, "Spontaneous Emission in a Periodic Structure", *Soviet Journal of Experimental and Theoretical Physics*, vol. 35, no. 6, pp. 269-273, 1972.

[4] Ohtaka, "Energy band of photons and low-energy photon diffraction", *Physical Review,* vol. 19, no.10, pp. 5057-5067, 1979.

[5] J. Ouellette, "Seeing the Future in Photonic Crystals", *The Industrial Physicist*, vol. 7, no. 6, pp. 14 -17, 2002.

[6] E.Yablonovitch, "Inhibited Spontaneous Emission in Solid-State Physics and Electronics", *Physical Review Letters*, vol. 58, no. 20, pp. 2059-2062, 1987.

[7] S. John, "Strong localization of photons in certain disordered dielectric super-lattices", *Physical Review Letters*, vol. 58, no. 23, pp. 2486-2489, 1987.

[8] T. F. Krauss, R. M. De La Rue, S. Brand, "Two-dimensional photonic band gap structures operating at near-infrared wavelengths", *Physical Review Letters*, vol. 383, no. 6602, pp. 699-702, 1996.

[9] Miguez, Meseguer, Ozin, Mondia, Francisco "Large-scale synthesis of a silicon photonic crystal with a complete three-dimensional bandgap near 1.5 micrometres", *Physical Review Letters*, vol. 405, no. 6785, pp. 437-440, 2000

[10] Ho, K. M., C. T. Chan, C. M. Soukoulis, "Existence of a photonic gap in periodic dielectric structures", *Phys. Rev. Lett.*, vol. 65, no. 11, pp 3152-3155, 1990.

[11] Jackson, J. D., *Classical Electrodynamics*, 3rd Edition. New York: Wiley, 1998.

[12] Bloembergen, *Nonlinear Optics*, 2nd edition. New York: W. A. Benjamin, 1965.

[13] S. G. Johnson and J. D. Joannopoulos, *Introduction to Photonic Crystals: Bloch's Theorem, Band Diagrams, and Gaps (But No Defects)*, 3rd Ed.: MIT, 2003.

[14] S. S. Mohammad, H. A. Banae , "Band gap properties of 2D square lattice photonic crystal composed of rectangular cells", *Optoelectron*, vol. 6, no. 3, pp. 346-352, 2013.

[15] K. S. Yee, "Numerical Solution of Initial Boundary Value Problems Involving Maxwell's Equation in Isotropic Media,", *IEEE Transactions on Antenna Propagation*, vol. 14, no. 3, pp. 302-307, 1996.

[16] Opti-FDTD Tutorials Finite Difference Time Domain Photonics, Simulation Software © 2013 Optiwave.

[17] J. D. Joannopoulos, P.R. Villeneuve, S. Fan, "Photonic Crystals: Putting a new twist on light", *Nature,* vol. 386, no.4, pp. 143, 1997.

[18] B. Jalali, S. Yegnanarayanan, T. Yoon, T. Yoshimoto, I. Rendina, F. Coppinger "Advances in Silicon-on-Insulator Optoelectronics", *IEEE Journal of Selected Topics in Quantum Electronics*, vol. 4, no. 6, pp. 938, 1998

[19] A. Ghafari, M. Javid, F. Monifi, M. S. Abrishamian, "A numeric analysis of photonic crystal tunable add-drop filters based on ring resonators", *IEEE Conference*, vol. 14, no. 2, pp 351, 2007

[20] A.Taalbi, G. Bassou, M.Y. Mahmoud, "New design of channel drop filters based on photonic crystal ring resonators", *Optik*, vol. 124, no. 5, pp. 824-827, 2013

[21] P. Andalib, N. Granpayeh, "Optical Add/drop Filter Based on Dual Curved Photonic Crystal Resonator", *IEEE*, vol.37, no. 1, pp 170, 2008

[22] W. Zhou, Z. Qiang, Richard A. Soref , "Optical Add-Drop Filter Design Based on Photonic Crystal Ring Resonators", *Optical Society of America*, vol. 39, no. 5, pp.1081- 1085, 2007

[23] J. R. Vivas, D. N. Chigrin, A. V. Lavrinenko, C. M. Torres, "Resonant add-drop filter based on a photonic quasi-crystal", *Optics Express, Optical Society of America*, vol. 13, no. 3, pp. 826, 2005.

[24] S. Robinson, R. Nakkeeran, "Two-dimensional Photonic Crystal Ring Resonator based Add Drop Filter for CWDM systems", *Optik*, vol. 124, no. 5, pp. 3430-3435, 2013.

[25] M. Djavid, M.S. Abrishamian, "Multi-channel drop filters using photonic crystal ring resonators", *Optik*, vol. 123, no. 5, pp. 167-170, 2012

[26] M. Y. Mahmouda, G. Bassoua, A. Taalbi, "A new optical add–drop filter based on two-dimensional photonic crystal ring resonator", *Optik*, vol. 124, no. 1, pp. 2864-2867, 2013

[27] R. Ahmed, Md. Masruf Khan, R. Ahmmed, A. Ahad, "Design, Simulation & Optimization of 2D Photonic Crystal Power Splitter", *Optics and Photonics Journal*, vol.3, no. 1, pp. 13-19, 2013

[28] J. Stewart, A. Pyayt, "Photonic crystal based microscale flow cytometry", *Optics Express*, vol. 22, no. 11, pp. 12853, 2014

[29] S. Dominguez, I. Cornago, O. Garcia, M. Ezquer, M.J. Rodriguez, A.R. Lagunas, J. Conde, J. Bravo, "Design, optimization and fabrication of 2D photonic crystals for solar cells", *Photonics and Nanostructures - Fundamentals and Applications*, vol. 11, no. 6, pp. 29-36, 2013

[30] G. Calo, V. Petruzzelli, "Wavelength routers for optical networks-on-chip using optimized photonic crystal ring resonators", *IEEE Journal of Photonics*, vol. 5, no. 3, pp. 1011, 2013

[31] S. Robinson, R. Nakkeeran, "PCRR Based Bandpass Filter for C and L+U Bands of ITU-T G.694.2 CWDM Systems", *Optics and Photonics Journal*, vol. 1, no. 3, pp. 145-149, 2011.

[32] K. Fasihi, S. Mohammad, "Orthogonal Hybrid Waveguides: An Approach to Low Crosstalk and Wideband Photonic Crystal Intersections Design", *Journal of Lightwave Technology*, vol. 27, no. 6, pp. 799, 2009.

[33] G. Lin, X. Chen, D. Zhuang, "1 × 4 optical multiplexer based on the self-collimation effect of 2D photonic crystal", Elsevier, vol. 30, no. 4026, pp. 546-550, 2014.

[34] W.Y. Chiu, T.W. Huang, Y.H. Wu, Y.J. Chan, C.H. Hou, H.T. Chien, C.C. Chen, "A photonic crystal ring resonator formed by SOI nano-rods", *Optical Express*, vol. 15, no. 23, pp. 155, 2007.

[35] K. D. Chang, C. Y. Liu, "Electro-optical channel drop switching in a photonic crystal waveguide-cavity side-coupling system", *Elsevier, Optics Communications*, vol. 316, no. 5, pp. 10-16, 2014.

[36] J. Bao, J. Xiao, L. Fan, X. Li, Yunfei Hai, Tong Zhang, Chunbo Yang, "All-optical NOR and NAND gates based on photonic crystal ring resonator", *Elsevier, Optics Communications,* vol. 329, no. 10, pp.109-112, 2014.

[37] W. Y. Chiu, T. W. Huang, Y. H. Wu, F. H. Huang, Y. J. Chan, C. H. Hou, H. T. Chien, C. Chen, S. H. Chen, and J. I. Chyi, "Directional Coupler Formed by Photonic Crystal InAlGaAs Nano-rods", *Journal of Lightwave Technology*, vol. 26, no. 5, pp. 488-491, 2008.

[38] S. Assefa, P. T. Rakich, P. Bienstman, S. G. Johnson, G. S. Petrich, J. D. Joannopoulos, L. A. Kolodziejski, E. P. Ippen, and H. I. Smith, "Guiding 1.5 μm light in photonic crystals based on dielectric rods", *Applied Physics Letters*, vol. 85, no. 25, pp. 6110, 2004.

[39] N. Zhu, Y. Wang, Q. Ren, Li Zhu, M. Yuan, Guimin, "Slow light in nonlinear photonic crystal coupled-cavity waveguides", *Optics & Laser Technology, Elsevier*, vol. 57, no. 28, pp. 154-158, 2013.

[40] A. Wirth Jr., A.S.B. Sombra, "Graphene-photonic crystal switch", *Optics Communications, Elsevier*, vol. 321, no. 15, pp. 150-156, 2014.

[41] E Pourali, M.K. Farshi, M. Heidari, "Design and analysis of slow light regime in silicon carbide 2D photonic crystal waveguides", *Infrared Physics & Technology, Elsevier*, vol. 63, no. 1, pp. 10-16, 2013.

[42] C. Sciancalepore, B. Ben Bakir, C. Seassal, X. Letartre, J. Harduin, N. Olivier, J.M. Fedeli, P. Viktorovitch, "Thermal, Modal, and Polarization Features of Double Photonic Crystal Vertical-Cavity Surface-Emitting Lasers", *IEEE Journal of Photonics*, vol. 4, no. 2, pp. 399, April 2012

[43] B. Kumar, V. Suthar, K. S. Kumar, A. Singh, "Tunable wavelength demultiplexer for DWDM applications using 1-D photonic crystal", *Progr. Electromag. Res. Lett*., vol. 33, no. 1, pp. 27-35, 2012.

[44] Y. J. Quan, P. D. Han, X. D. Lu, Z. C. Ye, Li Wu, "Optical interleaver based on directional coupler in a 2D photonic crystal slab with triangular lattice of air holes", *Optics Communications*, vol. 27, no. 11, pp. 203-206, 2007.

[45] F. Cuesta Soto, A. Martínez, J. Martí, "Experimental observation of intermodal dispersion in photonic crystal directional couplers", *Journal of Applied Physics*, vol. 104, no. 12, pp. 123107 - 123107-4, 2008.

[46] M. K. Moghaddam, A. Attari, M. Mirsalehi , "Improved photonic crystal directional coupler with short length", *Photonics and Nanostructures – Fundamentals and Applications*, vol.8, no. 2, pp. 47-53, 2010.

[47] Y. Xu, C. Caer, D. Gao, E. Cassan, X. Zhang, "High efficiency asymmetric directional coupler for slow light slot photonic crystal waveguides", *Optics Express* (*OSA)*, vol. 22, no.9, pp. 11021-11028, 2014.

[48] A. Yariv, "Coupled mode theory for guided-wave optics", *IEEE Journal Quantum Electron*, vol. 9, no. 9, pp. 919-933, 1973

[49] E. P. Kosmidou, E. E. Kriezis, and T. D. Tsiboukisc, "Analysis of tunable photonic crystal directional couplers", *Journal of Applied Physics*, vol. 100, no. 4, pp. 43118, 2006.

[50] F. Sulser, G. Poberaj, M. Koechlin, P. Gunter, "Photonic crystal structures in ion-sliced lithium niobate thin films", *OSA, Optics Express*, vol. 17, no. 22, pp. 20291-20300, 2009.

[51] G. keiser, *Optical communications essentials*, 2nd Ed.: McGraw Hill Companies Inc. United States of America, 2003.

[52] J. B. Pendry, "Calculating Photonic Band Structure", *Journal of Physics*: *Condensed Matter*, vol. 8, no. 9, pp. 1085-1108, 1996.

[53] S. Kuchinsky, V.Y. Golyatin, A.Y. Kutikov, T. P. Pearsall, and D. Nedeljkovic, "Coupling between photonic crystal waveguides", *IEEE Journal Of Quantum Electronics*, vol. 38, no. 10, pp. 1349, 2002.

[54] A. Taflove, *Computational Electrodynamics: The Finite-Difference Time-Domain Method*, 3rd Edition. London: Artech House, 2005.

[55] F.L. Hsiao, C. Lee, "Nanophotonic biosensors using hexagonal nanoring resonators: computational study", *SPIE*, vol. 10, no.1, pp. 013001-013001-8, 2011.

[56] T. N. Bakhvalova, I. V. Khmelnitsky, "Passive components based on two-dimensional photonic crystals", *Progress in Electromagnetics Research Symposium Proceedings, Moscow, Russia*, vol.8, no. 23, pp. 1143, 2012.

LIST OF PUBLICATIONS

[1] Harkiranjeet Kaur, R.S. Kaler, "Design and Analysis of 3-dB Photonic Crystal Directional Couplers", Communicated to Optik- International journal for light and electron.

[2] Harkiranjeet Kaur, R.S. Kaler, Balveer Painam, "Design of Photonic Crystal Add-Drop Filters Based on Quasi-Ring Cavities", Communicated to Optical Engineering, SPIE.

[3] Harkiranjeet Kaur, R.S. Kaler, "Design and Analysis of 2D Photonic Crystal Wavelength Routers using Micro-Ridge and Arc Waveguides", Communicated to Fiber and Integrated Optics.